A physically based distributed karst hydrological model (QMG model-V1.0) for flood simulation

Ji Li[1,*], Daoxian Yuan[1,2], Fuxi Zhang[3], Jiao Liu[4], Mingguo Ma[1]

[1]Chongqing Jinfo Mountain Karst Ecosystem National Observation and Research Station, Chongqing Key Laboratory of Karst Environment, School of Geographical Sciences, Southwest University, Chongqing 400715, China

[2]Key Laboratory of Karst Dynamics, MNR & Guangxi, Institute of Karst Geology, Chinese Academy of Geological Sciences, Guilin 541004, China

[3]College of Engineering Science and Technology, Shanghai Ocean University; Shanghai Engineering Research Center of Marine Renewable Energy 201306, China

[4]Chongqing municipal hydrological monitoring station, Chongqing 401120, China

Corresponding author: Ji Li (445776649@qq.com)

Abstract Karst trough and valley landforms are prone to flooding, primarily because of the unique hydrogeological features of karst landforms, which are conducive to the spread of rapid runoff. Hydrological models that represent the complicated hydrological processes in karst regions are effective for predicting karst flooding, but their application has been hampered by their complex model structures and associated parameter sets, especially for distributed hydrological models, which require large amounts of hydrogeological data. Distributed hydrological models for predicting flooding are highly dependent on distributed modelling processes, complicated boundary parameter settings, and extensive hydrogeological data processing steps, which are time consuming and computationally expensive. In this study, a distributed physically based karst hydrological model called the

QMG (Qingmuguan) model is proposed. The structural design of this model is relatively simple, and it is generally divided into surface and underground double-layered structures. The parameters that represent the structural functions of each layer have clear physical meanings, and fewer parameters are required than are need for other distributed models. This approach allows karst areas to be modelled with only a small amount of necessary hydrogeological data. Eighteen flood processes associated with the karst underground river in the Qingmuguan karst trough valley are simulated by the QMG model, and the simulated values agree well with observations, for which the average value of the Nash–Sutcliffe coefficient is 0.92. A sensitivity analysis shows that the infiltration coefficient, permeability coefficient, and rock porosity are the most important parameters in model calibration and optimization. The improved predictions of karst flooding obtained with the proposed QMG model enhance the mechanistic understanding of runoff generation and flow in karst trough valleys.

Keywords: Simulation and forecasting of karst floods; Karst trough valleys; QMG (Qingmuguan) model; Parametric optimization; Parameter sensitivity analysis

1 Introduction

Karst trough and valley landforms are very common in China, especially in the southwest. In general, these karst areas are water scarce during most of the year because their surfaces store very little rainfall, but they are also potential sources of floods because the local trough and valley landforms and topographic features facilitate the formation and propagation of floods (White, 2002; Li et al., 2021). The coexistence of drought and flood is a typical phenomenon in these karst trough and valley areas. For example, in the present study area, the Qingmuguan karst trough valley, floods were historically prevalent during the rainy season. In recent years, with more extreme rainfall events and the increased area of construction land in the region, rainfall infiltration has decreased, and rapid runoff over impervious surfaces has increased, resulting in frequent catastrophic flooding in the basin (Liu et al., 2009). Excess water flows from karst sinkholes and underground river outlets during floods (Jourde et al., 2007, 2014; Martinotti et al., 2017), flooding large areas of farmland and residential areas and causing serious economic losses (Gutierrez, 2010; Parise, 2010; Yu et al., 2020). Therefore, it is both important and urgent to simulate and predict karst flooding events in karst trough and valley regions, such as the study area.

Hydrological models can be effective for forecasting floods and evaluating water resources in karst areas (Bonacci et al., 2006; Ford and Williams, 2007; Williams, 2008, 2009). However, modelling floods in karst regions is extremely difficult because of the complex hydrogeological structures of these regions. Karst water-bearing systems consist of multiple media and are influenced by complex karst development dynamics (Worthington et al., 2000; Kovács and Perrochet, 2008; Gutierrez, 2010), such as karst caves, conduits, fissures and pores; thus, such systems are usually highly spatially heterogeneous (Chang and Liu, 2015; Teixeiraparente et al., 2019). In addition, the complex surface hydrogeological conditions and the hydrodynamic conditions inside karst water-bearing media result in significant temporal and spatial differences in the hydrological processes in karst areas (Geyer et al., 2008; Bittner et al., 2020).

In early studies of flood forecasting in karst regions, simplified lumped hydrological models were commonly used to describe the rainfall–discharge relationship (e.g., Kovács and Sauter, 2007; Fleury et al., 2007b; Jukić and Denić, 2009; Hartmann et al., 2014a). With the development of physical exploration technology and the progress made in mathematics, computing and other interdisciplinary disciplines, the level of modelling has gradually improved (Hartmann and Baker, 2017; Hartmann, 2018; Petrie et al., 2021). Subsequently, distributed hydrological models have been widely used in karst areas. The main difference between lumped and distributed hydrological models is that the latter divide the entire basin into many subbasins to simulate runoff generation and confluence characteristics, thereby effectively describing the physical properties of the hydrological processes that occur in karst water-bearing systems (Jourde et al., 2007; Hartmann, 2018; Epting et al., 2018).

Because of their simple structure and low demand for modelling data, lumped hydrological models have been used widely in karst areas (Kurtulus and Razack, 2007; Ladouche et al., 2014). In a lumped model, a river basin is considered as a whole when simulating runoff generation and flow paths, and there is no division into subbasins (Dewandel et al., 2003; Bittner et al., 2020). Lumped models usually consider the inputs and outputs of the study area (Liedl and Sauter, 2003; Hartmann and Bake, 2013, 2017). In addition, most of the model parameters are not optimized in a lumped model, and the physical meaning of each parameter may be unclear (Chen, 2009; Bittner et al., 2020).

Distributed hydrological models are of high interest in flood simulation and forecasting research (Ambroise et al., 1996; Beven and Binley, 2006; Zhu and Li, 2014). Compared with lumped models, distributed models provide clear physical meaning regarding the model structure and mechanisms (Meng and Wang, 2010; Epting et al., 2018). In a distributed hydrological model, an entire karst basin can be divided into many subbasins (Birk et al., 2005) using high-resolution digital elevation map (DEM) data. In the rainfall-runoff algorithm of a model, the hydrogeological conditions and karst aquifer characteristics can be fully considered to precisely simulate runoff generation and flow processes (Martinotti et al.,2017; Gang et al., 2019). Additionally, some basin-scale distributed hydrological models (not specific groundwater numerical models, such as MODFLOW) have been applied in karst areas, and they include the SHE/MIKE SHE model (Abbott et al., 1986a,b; Doummar et al., 2012), the SWMM model (Peterson and Wicks, 2006; Blansett and Hamlett, 2010; Blansett, 2011), TOPMODEL (Ambroise et al., 1996; Suo et al., 2007; Lu et al., 2013; Pan, 2014) and the SWAT model (Peterson and Hamlett, 1998; Ren, 2006).

The commonly used distributed hydrological models have various structures and numerous parameters (Lu et al., 2013; Pan, 2014), and a model may require vast amounts of data to build a framework for simulations in karst regions. For example, the distributed groundwater model MODFLOW-CFPM1 requires detailed data regarding the distribution of karst conduits in a study area (Reimann et al., 2009). Another example is the Karst–Liuxihe model (Li et al., 2019); notably, there are fifteen parameters and five underground vertical structures in the model. Such a complex structure increases the data demand, and modelling in karst areas is extremely difficult. In addition, a special borehole pumping test may be required to obtain the rock permeability coefficient.

To overcome the large data demands of distributed hydrological models in karst areas, a new physically based distributed hydrological model—known as the QMG (Qingmuguan) model-V1.0—was developed in the present study. Other commonly used karst groundwater models with complex structures and parameters, such as the aforementioned MODFLOW-CFPM1 model, require considerable hydrogeological data for modelling in karst areas (Qin and Jiang, 2014). The new QMG model has high potential for application in karst hydrological simulation and forecasting; it has certain advantages related to its framework and structural design, such as a double-layer structure and few parameters. The horizontal structure is divided into river channel units and slope units, and the vertical structure below the surface is divided into shallow karst aquifer and deep karst aquifer systems. This relatively simple model structure reduces the demand for modelling data in karst areas, and limited hydrogeological data are needed for modelling. To ensure that the QMG model works well in karst flood simulation and prediction despite its relatively simple structure and few parameters, we carefully designed the algorithms for runoff generation and flow in the model. Additionally, to verify the applicability of the QMG model in flood simulation in karst basins, we selected the Qingmuguan karst trough valley in Chongqing, China, as the study area for flood simulation and uncertainty analysis. In particular, we analysed the sensitivity of the model parameters.

2 Study area and data

2.1 Landform and topography

The Qingmuguan karst trough valley is located in the southeastern part of the Sichuan Basin, China, at the junction of the Beibei and Shapingba districts in Chongqing, with the coordinates 29°40′N–29°47′N and 106°17′E–106°20′E. The basin covers an area of 13.4 km^2 and is part of the southern extension of the anticline at Wintang Gorge in the Jinyun Mountains, with the anticlinal axis of Qingmuguan located in a parallel valley in eastern Sichuan (Yang et al., 2008). The surface of the anticline is heavily fragmented, and faults are extremely well developed with large areas of exposed Triassic carbonate rocks. Under the long-term erosion of karst water, a typical karst trough landform has formed, which looks like a pen-holder structure, means 'three ridges with two troughs' (Liu et al., 2009). This karst trough landform provides ideal conditions for flood propagation, and the development of karst landforms is extremely common in this karst region of Southwest China, especially in the karst region of Chongqing.

The basin is oriented in a narrow band of slightly curved arcs and is ~12 km long from north to south. The direction of the mountains in the region is generally consistent with the direction of the tectonic line. The map in Figure 1 gives an overview of the Qingmuguan karst basin.

Figure 1. The Qingmuguan karst basin.

2.2 Hydrogeological conditions

The Qingmuguan basin is located within the subtropical humid monsoon climate zone, with an average temperature of 16.5°C and an average precipitation of 1250 mm concentrated mainly from May–September. An underground river system has developed in the karst trough valley, with a length of 7.4 km, and the water supply of the underground river is mainly rainfall recharge (Zhang, 2012). Most of the precipitation collects in hillslope areas and flows into the karst depressions at the bottom of the trough valley, where it provides recharge to the underground river through dispersed infiltration via surface karst fissures and sinkholes (Fig. 1a). An upstream surface river forms in a gentle valley and enters the underground river through the Yankou sinkhole (elevation 524 m). Surface water in the middle and lower reaches of the river system enters the underground river system mainly through cover-collapse sinkholes (Gutierrez et al., 2014) and fissures.

The stratigraphic and lithological characteristics of the basin are dominated largely by carbonate rocks of the Lower Triassic Jialingjiang Group (T_{1j}) and Middle Triassic Leikou Slope Group (T_{2l}) on both sides of the slope, with some quartz sandstone and mudstone outcrops of the Upper Triassic Xujiahe Group (T_{3xj}) (Zhang, 2012). The topography of the basin presents a general anticline (Fig. 1b), where carbonate rocks on the surface are corroded and fragmented and have high permeability. Compared with the core of the anticline, the shale of the anticline is less eroded and forms a good waterproof layer.

To investigate the distribution of karst conduits in the underground river system, we conducted a tracer test in the study area. The tracer was placed into the Yankou sinkhole and recovered in the Jiangjia spring (Fig. 1a,c). According to the tracer test results (Gou et al., 2010), the karst water-bearing medium in the aquifer was anisotropic, the karst conduits in the underground river were extremely well developed, and there was a large single-channel underground river approximately five metres wide. The response of the underground river to rainfall was very fast, with the peak flow observed at the outlet of Jiangjia spring 6–8 h after rainfall based on the tracer test results. The flood peak rose quickly, and the duration of the peak flow was short. The underground river system in the study area is dominated by large karst conduits, which are not conducive to water storage in water-bearing media but are very conducive to the propagation of floods.

2.3 Data

To build the QMG model to simulate karst flood events, the necessary modelling baseline data had to be collected, and they included 1) high-resolution DEM data and hydrogeological data (e.g., the thickness of the epikarst zone, rainfall infiltration coefficient for different karst landforms, and permeability coefficient of rock); 2) land use and soil type data; and 3) rainfall data in the basin and water flow data for the underground river. The DEM data were downloaded from a free internet database and had an initial spatial resolution of 30 × 30 m. The spatial resolution of the land use and soil type data was 1000 × 1000 m, and these data were also downloaded from the internet. After considering the applicability and computational strength of the model, as well as the size of the basin in the study area (13.4 km^2), the spatial resolution of the three types of data was resampled uniformly in the QMG model and downscaled to 15 × 15 m based on the spatial discrete method proposed by Berry et al. (2010).

The hydrogeological data necessary for modelling were obtained in three simple ways. 1) A basin survey was conducted to obtain the thickness of the epikarst zone, which was achieved by observing the rock formations on hillsides following cutting for road construction. Information was collected regarding the location, general shape, and size of karst depressions and sinkholes, and these data were combined with DEM data and used to determine the convergence process of these depressions. The sinkholes in the basin are cover-collapse sinkholes (Gutierrez et al., 2014) according to the basin survey. There are 3 large sinkholes (more than 3 metres in diameter) and 12 small sinkholes (less than 1 metre in diameter). The rest of the sinkholes, 5 in total, are between 1 and 3 metres in diameter. The confluence calculations for sinkholes in the model were based on the results of a previous study (Meng et al., 2009). 2) Empirical equations developed for similar basins were used to obtain the rainfall infiltration coefficient for different karst landforms and the permeability coefficient of rock. For example, the rock permeability coefficient was calculated based on an empirical equation established based on a pumping test in a coal mine in the study area (Li et al., 2019, 2022). 3) A tracer experiment was conducted in the study area (Gou et al., 2010) to obtain information on the underground flow direction and flow velocity; for instance, underground karst conduits are well developed in the area, and an underground river approximately five metres wide is present. There is no hydraulic connection between the underground river system in the area and the adjacent basin, which means that there is no overflow recharge.

Rainfall and flood data are important model inputs and represent the driving factors of hydrological models. In the study area, rainfall data were acquired with two rain gauges located in the basin (Fig. 1a). Point rainfall was then spatially interpolated to obtain basin-level rainfall (for such a small basin area, the rainfall results obtained from two rain gauges were considered representative). There were 18 karst flood events from 14 April 2017 to 10 June 2019. We built a rectangular open channel at the underground river outlet and set up a river gauge in the channel (Fig. 1a) to record the water level and flow data every 15 minutes.

3 Methodology

3.1 Hydrological model framework and algorithms

The hydrological model developed in this study was named the QMG model after the basin for which it was developed and to which it was first applied, i.e., the Qingmuguan basin. The QMG model has a two-layer structure, including a surface part and an underground part. The surface part mainly performs the runoff generation and surface routing calculations, and the underground part performs the routing calculations for the underground river system.

The structure of the QMG model is divided into a two-layer structure with horizontal and vertical components. The horizontal structure of the model is divided into river channel units and slope units. The vertical structure below the surface is divided into a shallow karst aquifer (including soil layers, karst fissures and conduit systems in the epikarst zone) and a deep karst aquifer system (bedrock and underground river system). With this relatively simple model structure, only a small amount of hydrogeological data is needed in karst regions. Figure 2 shows a flowchart of the modelling and calculation procedures required for the QMG model.

Figure 2. Modelling flow chart of the QMG (Qingmuguan) model.

To accurately show the runoff generation and routing processes at the grid scale, the karst subbasins are further divided into many karst hydrological response units (KHRUs) based on the high-resolution (15 × 15 m) DEM data in the model. The specific steps involved in the division were adopted by referring to a study of hydrological response units (HRUs) in TOPMODEL by Pan (2014). As the smallest basin units for computing, KHRUs can effectively mitigate the spatial differences in karst development within units and reduce the uncertainty in the classification of model units. Figure 3 shows the spatial structure of the KHRUs.

Figure 3. Spatial structure of karst hydrological response units (KHRUs) (Li et al., 2021).

The right-hand side of Figure 3 shows a three-dimensional spatial model of KHRUs established in the laboratory to visually reflect the storage and movement of water in a karst water-bearing medium with spatial anisotropy and to provide technical support for establishing the hydrological model.

The modelling and operation of the QMG model involve three main stages: 1) spatial interpolation and the establishment of rainfall and evaporation calculations; 2) runoff generation and routing calculations for the surface river; and 3) routing calculations for underground runoff, including in the shallow karst aquifer and the underground river system.

3.1.1 Rainfall and evaporation calculations

In the QMG model, the spatial interpolation of rainfall is accomplished with a kriging method using ArcGIS 10.2 software. In some cases, the Thiessen polygon method may be a simpler method for rainfall interpolation if the number of rainfall gauges in the basin is sufficient. The point rainfall observed with the two rainfall gauges in the basin (Fig. 1a) was interpolated spatially into areal rainfall for the entire basin.

Basin evapotranspiration in the KHRUs was mainly from vegetation, the soil and water surfaces. These evapotranspiration components were calculated using the following equations (modified from Li et al., 2020):

$$\begin{cases} E_v = V^{t+\Delta t} - V^t - P_v \\ E_s = \lambda E_p, \text{if } F = F_c \\ E_s = \lambda E_p \dfrac{F}{F_c}, \text{if } F < F_{\text{sat}} \\ E_w = \Delta e \cdot \left[1.12 + 0.62\left(\Delta T\right)^{0.9}\right] \cdot \left[0.084 + 0.24\left(1-\gamma^2\right)^{1/2}\right] \cdot \left[0.348 + 0.5\omega^{1.8\text{-}1.137\omega^{0.05}}\right] \end{cases} \tag{1}$$

where E_v [mm] is the vegetal discharge, $V^{t+\Delta t} - V^t$ [mm] is the rainfall variation due to vegetation interception, P_v [mm] is the interception of rainfall by vegetation and E_s [mm] is the actual soil evaporation. The term λ is the evaporation coefficient. The term E_p [mm] is potential evaporation, which can be measured experimentally or estimated with a water surface evaporation equation for E_w. The term F [mm] is the actual soil moisture, F_{sat} [mm] is the saturation moisture content, F_c [mm] is the field capacity, E_w [mm/d] is the evaporation from a water surface and $\Delta e = e_0 - e_{150}$ [hPa] is the draught head between the saturation vapour pressure of a water surface and the air vapour pressure 150 m above the water surface. The term $\Delta T = t_0 - T_{150}$ [°C] is the temperature difference between a water surface and a location 150 m above the water surface, γ is the relative humidity 150 m above the water surface and ω [m/s] is the wind speed 150 m above the water surface.

3.1.2 Runoff generation

In the QMG model, the surface runoff generation in river channel units is associated with the rainfall in the basin that enters the river system after subtracting evaporation losses. This portion of the runoff is directly involved in the routing process through the river system rather than undergoing infiltration. In contrast, the process of runoff generation in slope units is more complex and related to the developmental characteristics of the surface karst features in the basin, the rainfall intensity and soil moisture. For example, when the soil is saturated, there is the potential for excess infiltration-based surface runoff in exposed karst slope units. Surface runoff generation in river channel units and slope units in KHRUs can be described by the following equations (modified from Chen, 2009, 2018; Li et al., 2020):

$$\begin{cases} P_r(t) = \left[P_i(t) - E_p \right] \dfrac{L \cdot W_{\max}}{A} \\ R_{\mathrm{si}} = (P_i - f_i), P_i \geq f_{\max} \\ R_{\mathrm{si}} = 0, P_i < f_{\max} \\ f_{\max} = \alpha (F_{\mathrm{c}} - F)^{\beta} + F_s \end{cases} \tag{2}$$

where $P_r(t)$ [mm] is the net rainfall (subtracting evaporation losses) in the river channel units at time t [h], $P_i(t)$ [mm] is the rainfall in the river channel units, L [m] is the length of the river channel, $W_{\max}$ [m] is the maximum width of the river channel selected and A [m^2] is the cross-sectional area of the river channel. R_{si} [mm] is the excess infiltration runoff in the QMG model when the vadose zone is nonsaturated. Notably, the infiltration capacity $f_{\max}$ varies in different karst landform units. α and β are the parameters of the Holtan model, and F_{s} [mm] is the stable depth of soil water infiltration.

In the KHRUs (Fig. 3), underground runoff is generated primarily from the infiltration of rainwater and direct confluence recharge from sinkholes or karst windows. In the QMG model, underground runoff is calculated by the following equations (modified from Chen, 2018):

$$\begin{cases} R_g = R_0 \exp(-pt^m) \\ R_e = v_e \cdot I_\mathrm{w} \cdot z \end{cases} \tag{3}$$

where

$$\begin{cases} \dfrac{\partial R_e}{\partial x} + I_\mathrm{w} \cdot z \cdot \dfrac{\partial F}{\partial t} = R_\mathrm{r} - R_\mathrm{epi} \\ v_e = K \cdot \tan(\alpha), \quad F > F_\mathrm{c} \\ v_e = 0, \quad F \le F_\mathrm{c} \end{cases} \tag{4}$$

Here, R_g [mm] is the underground runoff depth (this part of underground runoff is mainly directly from karst sinkholes or karst windows in the study area), R_0 [mm] is the average depth of underground runoff, p and m are attenuation coefficients that were calculated by conducting a tracer test in the study area, R_e [L/s] is the underground runoff generated from rainfall infiltration in the epikarst zone, I_w [mm] is the width of the underground runoff zone in the KHRUs, z [mm] is the thickness of the epikarst zone, R_r [mm^2/s] is the runoff-based recharge in the KHRUs during period t, R_epi [mm^2/s] is the water infiltration from rainfall, v_e [mm/s] is the flow velocity of underground runoff, K [mm/s] is the permeability coefficient and α is the hydraulic gradient of underground runoff. If the soil moisture level is less than the field capacity, $F \le F_\mathrm{c}$, and the vadose zone is not yet full, there will be no underground runoff generation, and rainfall infiltration will fill the vadose zone before it becomes saturated, at which point runoff is generated.

3.1.3 Channel routing and convergence

In the QMG model, runoff routing in KHRUs includes the confluence of the surface river channel and underground runoff. There are already many classic algorithms available for performing runoff routing calculations in river channel units and slope units, such as the Saint-Venant equations and Muskingum convergence model. In this study, the Saint-Venant equations were adopted to assess flow routing for the surface river and in hill slope units, and a wave movement equation was adopted for convergence calculations in slope units (Chen, 2009):

$$\begin{cases} \dfrac{\partial Q}{\partial x} + L\dfrac{\partial h}{\partial t} = q \\ S_f - S_0 = 0 \end{cases} \tag{5}$$

where

$$Q = vhL = \frac{L}{n} h^{\frac{5}{3}} S_0^{\frac{1}{2}} \tag{6}$$

Here, we customized two variables *a* and *b*:

$$\begin{cases} a = \left(\dfrac{n}{L} S_0^{-\frac{1}{2}}\right)^{\frac{3}{5}} \\ b = \dfrac{3}{5} \end{cases} \tag{7}$$

Equation (7) was substituted into Eq. (5) and discretized with a finite-difference method, yielding

$$\begin{cases} \dfrac{\partial Q}{\partial x} + abQ^{(b-1)} \dfrac{\partial Q}{\partial t} - q = 0 \\ \dfrac{\Delta t}{\Delta x} Q_{i+1}^{t+1} + a(Q_{i+1}^{t+1})^b = \dfrac{\Delta t}{\Delta x} Q_i^{t+1} + a(Q_{i+1}^{t})^b + q_{i+1}^{t+1}\Delta t \end{cases} \tag{8}$$

The Newton–Raphson method was used for the iterative calculation using Eq. (8):

$$\left[Q_{i+1}^{t+1}\right]^{k+1} = \left[Q_{i+1}^{t+1}\right]^{k} - \frac{\dfrac{\Delta t}{\Delta x}\left[Q_{i+1}^{t+1}\right]^{k} + a\left(\left[Q_{i+1}^{t+1}\right]^{k}\right)^{b} - \dfrac{\Delta t}{\Delta x} Q_i^{t+1} - a(Q_{i+1}^{t})^b - q_{i+1}^{t+1}\Delta t}{\dfrac{\Delta t}{\Delta x} + ab\left(\left[Q_{i+1}^{t+1}\right]^{k}\right)^{b-1}} \tag{9}$$

where Q [L/s] is the convergence of water flow in slope units, L [dm] is the width of the runoff zone in a slope unit, h [dm] is the runoff depth and q [dm^2/s] is the lateral inflow in the KHRUs. Here, the friction slope S_f equals the hill slope S_0, and the inertia term and the pressure term in the motion equation of the Saint-Venant equation set were ignored. The term v [dm/s] is the flow velocity of surface runoff in the slope units, as calculated by the Manning equation. Additionally, n is the roughness coefficient of the slope units, Q_i^{t+1} [L/s] is the slope inflow in a KHRU at time t+1 and Q_{i+1}^{t+1} [L/s] is the slope discharge in the upper adjacent KHRU at time t+1.

Similarly, surface river channel convergence was described based on the Saint-Venant equations, and a diffusion wave movement equation was adopted; therefore, the inertia term in the motion equation was ignored:

$$\begin{cases} \dfrac{\partial Q}{\partial x} + \dfrac{\partial A}{\partial t} = q \\ S_f = S_0 - \dfrac{\partial h}{\partial x} \end{cases} \tag{10}$$

A finite-difference method and the Newton–Raphson method were used to iteratively solve the above equation set:

$$\begin{cases} \left[Q_{i+1}^{t+1}\right]^{k+1} = \left[Q_{i+1}^{t+1}\right]^{k} - \dfrac{\dfrac{\Delta t}{\Delta x}\left[Q_{i+1}^{t+1}\right]^{k} + c\left(\left[Q_{i+1}^{t+1}\right]^{k}\right)^{b} - \dfrac{\Delta t}{\Delta x} Q_{i}^{t+1} - c\left(Q_{i+1}^{t}\right)^{b} - q_{i+1}^{t+1}\Delta t}{\dfrac{\Delta t}{\Delta x} + cb\left(\left[Q_{i+1}^{t+1}\right]^{k}\right)^{b-1}} \\ c = \left(\dfrac{1}{3600} n \chi^{\frac{2}{3}} S_f^{-\frac{1}{2}}\right)^{\frac{3}{5}} \end{cases} \tag{11}$$

where Q [L/s] is the water flow in surface river channel units, A [dm^2] is the cross-sectional area of discharge, c is a custom intermediate variable and χ [dm] is the wetted perimeter of the discharge cross-section.

The underground runoff area in the model includes the convergence region of the epikarst zone and underground river. In the epikarst zone, the karst water-bearing media are highly heterogeneous (Williams, 2008). For example, anisotropic karst fissure systems and conduit systems consist of corrosion fractures. When rainfall infiltrates into the epikarst zone, water moves slowly through the small (less than 10 cm in this study) karst fissure systems, and it flows rapidly in larger (more than 10 cm) conduits. The key to estimating the flow velocity lies in determining the width of karst fractures. In the KHRUs (Fig. 3), a fracture width of 10 cm was used as a threshold value (Atkinson, 1977) based on a borehole pumping test in the basin. Thus, if the fracture width exceeded 10 cm, then the water movement in the fracture was defined as rapid flow; otherwise, it was defined as slow flow. The flow in the epikarst zone was calculated by the following equation (modified from Beven and Binley, 2006):

$$Q(t)_{\mathrm{ijk}} = b_{\mathrm{ijk}} \cdot \frac{\Delta h}{\Delta l} R_i C_j \cdot T(t)_{\mathrm{slow/rapid}} \tag{12}$$

where

$$\begin{cases} T(t)_{\mathrm{slow}} = nr\dfrac{\rho g R_i C_j L_k}{12v} \\ T(t)_{\mathrm{rapid}} = \dfrac{K_{ij}\left(e^{-f_{ij}h_{ij}} - e^{-f_{ij}z_{ij}}\right)}{f_{ij}} \end{cases} \tag{13}$$

Here, $Q(t)_{ijk}$ [L/s] is the flow in the epikarst zone at time *t*, b_{ijk} [dm] is the width of the runoff zone, $\frac{\Delta h}{\Delta l}$ is the dimensionless hydraulic gradient, $T(t)_{\mathrm{slow/rapid}}$ is the dimensionless hydraulic conductivity, ρ [g/L] is the density of water, *g* [m/s^2] is gravitational acceleration, *n* is the number of valid computational units, $R_i C_j L_k$ [L] is the volume of the *ijk*-th KHRU, v is the kinematic viscosity coefficient, f_{ij} is the attenuation coefficient in the epikarst zone, h_{ij} [dm] is the depth of shallow groundwater and z_{ij} [dm] is the thickness of the epikarst zone.

The distinction between rapid and slow flows in the epikarst zone is not absolute. Notably, the established fracture threshold of 10 cm may be underrepresentative because pumping tests were conducted in only five boreholes in the region. In fact, there is usually water exchange between the rapid and slow flow zones at the junctions of large and small fissures in karst aquifers. In the QMG model, this water exchange can be described with the following equation (modified from Li et al., 2021):

$$\begin{cases} Q = \alpha_{i,j,k}\left(h_n - h_{i,j,k}\right) \\ \alpha_{i,j,k} = \displaystyle\sum_{ip=1}^{np} \frac{\left(K_w\right)_{i,j,k} \pi d_{ip} \frac{1}{2}\left(\Delta l_{ip} \tau_{ip}\right)}{r_{ip}} \end{cases} \tag{14}$$

Here, $\alpha_{i,j,k}$ [dm^2/s] is the water exchange coefficient in the *ijk*-th KHRU, $\left(h_n - h_{i,j,k}\right)$ [dm] is the water head difference between the rapid and slow flow zones at the junction of large and small fissures in KHRUs, *np* is the number of fissure systems connected to the adjacent conduit systems, $\left(K_w\right)_{i,j,k}$ [dm/s] is the permeability coefficient at the junction of a fissure and conduit, d_{ip} and r_{ip} [dm] are the conduit diameter and radius, respectively Δl_{ip} [dm] is the length of the connection between conduits *i* and *p*, and τ_{ip} is the conduit curvature. Some of the parameters in this equation, such as $\left(K_w\right)_{i,j,k}$ and $\left(h_n - h_{i,j,k}\right)$, were obtained by conducting an infiltration test in the study area.

The convergence patterns in the underground river system have an important influence on the flow regime at the basin outlet. To facilitate the routing calculations in the QMG model, the underground river system can be generalized into large multiple-conduit systems. During floods, these conduit systems are mostly under pressure. Whether the water flow is laminar or turbulent depends on the flow regime at that time. The water flow into these conduits is calculated based on the Hagen–Poiseuille equation and the Darcy–Weisbach equation (Shoemaker et al., 2008):

$$\begin{cases} Q_{\text{laminar}} = -A\dfrac{gd^2\partial h}{32\nu\partial x} = -A\dfrac{\rho g d^2 \Delta h}{32\mu\tau\Delta l} \\[2ex] Q_{\text{turbulent}} = -2A\sqrt{\dfrac{2gd\left|\Delta h\right|}{\Delta l\tau}}\log\left(\dfrac{H_c}{3.71d} + \dfrac{2.51\nu}{d\sqrt{\dfrac{2gd^3\left|\Delta h\right|}{\Delta l\tau}}}\right)\dfrac{\Delta h}{\left|\Delta h\right|} \end{cases} \tag{15}$$

Here, Q_{laminar} [L/s] is the laminar flow in the conduit systems, *A* [dm^2] is the conduit cross-sectional area, *d* [dm] is the conduit diameter, ρ [kg/dm^3] is the density of water, $\nu = \mu / \rho$ is the coefficient of kinematic viscosity, $\Delta h / \tau\Delta l$ is the hydraulic slope of the conduits, τ is the dimensionless conduit curvature, $Q_{\text{turbulent}}$ [L/s] is the turbulent flow in the conduit systems and H_c [dm] is the average conduit wall height.

3.2 Parameter optimization

In total, the QMG model has 12 parameters, of which flow direction and slope are topographic parameters that can be determined from the DEM without parametric optimization, and the remaining 10 parameters require calibration. Other distributed hydrological models with multiple structures usually have many parameters. For example, the Karst–Liuxihe model (Li et al., 2021) has 15 parameters that must be calibrated. In the QMG model, each parameter is normalized as

$$x_i = x^*_i / x_{i0}, \tag{16}$$

where x_i is the dimensionless parameter value for i after it is normalized, x^*_i is the parameter value for i in actual physical units, and x_{i0} is the initial or final value of x_i. Through the processing of Eq. (16), the value range of the model parameters is limited to a hypercube $K_n = (X \mid 0 \le x_i \le 1, \ i = 1, 2, ..., n)$, and K is a dimensionless value. This normalization process ignores the influence of the spatiotemporal variation in the underlying surface attributes on the parameters while also simplifying parameter classification and the number of model parameters to a certain extent. Accordingly, the model parameters can be further divided into rainfall-evaporation parameters, epikarst zone parameters and underground river parameters. Table 1 lists the parameters of the QMG model.

Table 1. Parameters of the QMG model.

Because the QMG model has relatively few parameters, it is possible to calibrate them manually, which is easy and does not require a special program for parameter optimization. However, the disadvantage is that this manual approach is subjective, which can lead to uncertainty in the manual parameter calibration process. To compare the effects of parameter optimization on model performance, both manual parameter calibration and the improved chaotic particle swarm optimization algorithm (IPSO) were used for the automatic calibration of model parameters, and the effects of both on flood simulation were compared.

In general, the structure and parameters of a standard particle swarm optimization algorithm (PSO) are simple, with the initial parameter values obtained at random. For parameter optimization in high-dimensional multipeak hydrological models, the standard PSO is easily limited to local convergence and cannot achieve the optimal effect, and the late evolution of the algorithm may also cause problems, such as premature convergence or stagnant evolution, due to the ‘inert’ aggregation of particles, which seriously affects the efficiency of parameter selection. It is necessary to overcome the above problems so that the algorithm can converge to the global optimal solution with a high probability. In parameter optimization for the QMG model, we improved the standard PSO algorithm by adding chaos theory and developed the IPSO method; notably, 10 cycles of chaotic disturbances were added to improve the activity of the particles. The inverse mapping equation for the chaotic variable is

$$\begin{cases} X_{ij} = X_{\min} + (X_{\max} - X_{\min}) * Z_{ij} \\ Z_{ij}^{'} = (1-\alpha)Z^{*} + \alpha Z_{ij} \end{cases} \tag{17}$$

where X_{ij} is the optimization variable for the model parameters, $(X_{\max} - X_{\min})$ is the difference between the maximum and minimum values of X_{ij}, Z_{ij} is the variable before the disturbance is added, $Z^{'}_{ij}$ is the chaotic variable after a disturbance is added, α is a variable determined by the adaptive algorithm ($0 \leq \alpha \leq 1$), and Z^{*} is the chaotic variable formed when the optimal particle is mapped to the interval [0,1]. The flowchart of IPSO is shown in Figure 4.

Figure 4. Algorithm flow chart of IPSO.

3.3 Uncertainty analysis

Uncertainties in hydrological model simulation results usually originate from three factors: the input data, the model structure and the model parameters (Krzysztofowicz, 2014). In the present study, the input data (e.g., rainfall, flood and hydrogeological data) were first validated and preprocessed based on observations to reduce uncertainty.

Second, we simplified the structure of the QMG model to reduce the structural uncertainty. As a mathematical and physical model, a hydrological model is characterized by some uncertainty in flood simulation and forecasting because of the errors in the system structure and selected algorithm (Krzysztofowicz and Kelly, 2000). The model in this study was designed with full consideration of the relationship between the amount of data required to build the model and model performance in flood simulation and forecasting in karst regions. The entire model framework was integrated through simple structures and easy-to-implement algorithms based on the concept of distributed hydrological modelling. Conventionally, the level of uncertainty increases with the growing complexity of the model structure. We therefore ensured that the structure of the QMG model was simple when it was designed, and the double-layer model was divided into surface and underground structures to reduce structural uncertainty.

Third, we focused on analysing the uncertainty and sensitivity of model parameters and the applied optimization method; specifically, a multiparametric sensitivity analysis method (Choi et al., 1999; Li et al., 2020) was used to analyse the sensitivity of the parameters in the QMG model. The steps in the parameter sensitivity analysis are as follows.

1) Selection of the appropriate objective function

The Nash–Sutcliffe coefficient is widely used to evaluate the performance of hydrological models (Li et al., 2020, 2021); therefore, it was used to assess the QMG model in this study. Because the most important factor in flood forecasting is the peak discharge, it is used in the Nash coefficient equation:

$$NSC = 1 - \frac{\sum_{i=1}^{n}\left(Q_i - Q_i^{'}\right)^2}{\sum_{i=1}^{n}\left(Q_i - \overline{Q}\right)^2}, \tag{18}$$

where NSC is the Nash–Sutcliffe coefficient, Q_i [L/s] is the observed flow discharge, Q_i' [L/s] is the simulated discharge, $\overline{Q}$ [L/s] is the average observed discharge and n [h] is the observation period.

2) Parameter sequence sampling

The Monte Carlo sampling method was used to sample 8000 groups of parameter sequences. The parametric sensitivity of the QMG model was analysed and evaluated by comparing the differences between the a priori and a posteriori distributions of the parameters.

3) Parameter sensitivity assessment

The a priori distribution of a model parameter is its probability distribution, and the a posteriori distribution refers to the conditional distribution calculated after sampling, which can be calculated based on the results of parameter optimization. If there is a significant difference between the a priori distribution and the a posteriori distribution of a parameter, then the parameter being tested is characterized by high sensitivity; conversely, if there is no obvious difference, then the parameter is insensitive. The a priori distribution of a parameter is calculated as

$$\begin{cases} P_{i,j}(NSC_{i,j} \geq 0.85) = \dfrac{n}{N+1} \times 100 \\ \sigma_i = \sum_{j=1}^{n} \left(P_{i,j} - \overline{P_{i,j}} \right)^2 \end{cases} \tag{19}$$

where $P_{i,j}$ is the probability associated with a given a priori distribution when $NSC_{i,j} \geq 0.85$. We used a simulated Nash coefficient of 0.85 as the threshold value, and n was the number of occurrences of a Nash coefficient greater than 0.85 in flood simulations. In each simulation, only a certain parameter was changed, and the remaining parameters remained unchanged. If the Nash coefficient of a simulation exceeded 0.85, then the flood simulation results were considered acceptable. The term σ_i is the difference between an acceptable value and the overall mean, which represents the parametric sensitivity ($0 < \sigma_i < 1$). The higher the σ_i value is, the more sensitive the parameter. In this study, N denotes the 8000 parameter sequences, and $\overline{P_{i,j}}$ is the average value of the a priori distribution.

3.4 Model settings

After the model was built and before it was run, some of the initial conditions, such as the basin division scheme, the initial soil moisture levels, and the initial parameter ranges, were set. 1) In the study area, the entire Qingmuguan karst basin was divided into 893 KHRUs, including 65 surface river units, 466 hill slope units, and 362 underground river units. The division of these units formed the basis for runoff generation and convergence calculations. 2) The initial soil moisture level was set to 0–100% of the saturated moisture content in the basin, and the specific soil moisture level before each flood was determined through a trial calculation. 3) The hydraulic head boundary conditions for the groundwater zone were determined by a tracer test in the basin, and a perennial stable water level in area adjacent to the groundwater divide was used as the fixed head value at the model boundary. The base flow of the underground river was determined to be 35 L/s based on the perennial average dry season runoff. 4) The ranges of initial parameters and the convergence conditions were set before parameter optimization (Figure 4). 5) Parameter optimization and flood simulation were performed to validate the performance of the QMG model in karst basins.

4 Results and discussion

4.1 Parameter sensitivity results

The number of parameters in a distributed hydrological model is generally large, and it is important to perform a sensitivity analysis of each parameter to quantitatively assess the impact of the different parameters on model performance. In the QMG model, each parameter was divided into four categories according to its sensitivity: (i) highly sensitive, (ii) sensitive, (iii) moderately sensitive, and (v) insensitive. In the calibration of model parameters, insensitive parameters do not need to be calibrated, which can greatly reduce the number of calculations and improve the efficiency of model operations.

The flow process in the calibration period (14 April to 10 May 2017) was adopted to calculate the sensitivity of the model parameters, and calculations were based on equation (19). The parameter sensitivity results are listed in Table 2.

Table 2 Parametric sensitivity results for the QMG model.

In Table 2, the value of σ_i [equation (19)] represents a parameter's sensitivity, and the higher the value is, the more sensitive the parameter. The results in Table 2 indicate that the rainfall infiltration coefficient, rock permeability coefficient, rock porosity, and parameters related to the soil water content, such as the saturated water content and field capacity, are sensitive parameters. The order of parameter sensitivity is as follows: infiltration coefficient > permeability coefficient > rock porosity > specific yield > saturated water content > field capacity > flow direction > thickness > slope > soil coefficient > channel roughness > evaporation coefficient.

In the QMG model, parameters are classified as highly sensitive, sensitive, moderately sensitive, and insensitive according to their influence on the flood simulation results. In Table 4, we divide the sensitivity of model parameters into four levels based on the σ_i value: 1) highly sensitive parameters, $0.8 < \sigma_i < 1$; 2) sensitive parameters, $0.65 < \sigma_i < 0.8$; 3) moderately sensitive parameters, $0.45 < \sigma_i < 0.65$; and 4) insensitive parameters, $0 < \sigma_i < 0.45$. The highly sensitive parameters are the infiltration coefficient, permeability coefficient, rock porosity, and specific yield. The sensitive parameters are the saturated water content, field capacity, and thickness of the epikarst zone. The moderately sensitive parameters are the flow direction, slope, and soil coefficient. The insensitive parameters are channel roughness and the evaporation coefficient.

4.2 Parametric optimization

In total, the QMG model includes 12 parameters, of which only eight need to be optimized, which is relatively few for distributed models. The flow direction and slope, as channel roughness and the evaporation coefficient, which are insensitive parameters, need not be calibrated; this approach can improve the convergence efficiency of the model parameter optimization process.

In the study area, 18 karst floods from 14 April 2017 to 10 June 2019 were recorded at the underground river outlet to validate the effects of the QMG model in karst hydrological simulations. The calibration period was 14 April to 10 May 2017 at the beginning of the flow process, with the remainder of the period used as the validation period. In the QMG model, the IPSO algorithm was used to optimize the model parameters. To demonstrate the need for parameter optimization for the distributed hydrological model, the flood simulation results obtained using the initial parameters of the model (without parameter calibration) and the optimized parameters were compared. Figure 5 shows the iterative parameter optimization process for the QMG model.

Figure 5 Iterative parameter optimization process.

Figure 5 shows that almost all parameters considerably fluctuate at the beginning of the optimization, and after approximately 15 iterative optimization calculations, most of the linear fluctuations become significantly less variable, which indicates that the algorithm tends to converge (possibly only locally). When the number of iterations exceeded 25, all parameters remain essentially unchanged, suggesting that the algorithm converged (at this point, global convergence was achieved). It took only 25 iterations to achieve definite convergence for parameters in the applied IPSO algorithm; thus, this approach is extremely efficient in terms of parameter optimization for distributed hydrological models. In previous studies of the optimization of the parameters of the Karst-Liuxihe model in similar basin areas, 50 iterative steps were required to reach convergence in automatic parameter optimization (Li et al., 2021), demonstrating the effectiveness of the IPSO algorithm.

To evaluate the effect of parameter optimization, the convergence efficiency of the algorithm and, more importantly, the parameters after calibration were assessed in flood simulation cases. Figure 6 shows the flood simulation results.

Figure 6 Flow simulation results of the QMG model based on parameter optimization.

Figure 6 shows that the flows simulated following parameter optimization were better than those obtained with the initial model parameters. The simulated flow values based on the initial parameters were relatively small, with the simulated peak flows being notably smaller than the observed values; additionally, there were large errors between the simulated and observed values. In contrast, the simulated flows produced by the QMG model after parameter optimization were very similar to the observed values, which indicates that calibration of the model parameters was necessary and that there was an improvement in parameter optimization achieved through the use of the IPSO algorithm in this study. In addition, the flow simulation effect was better in the calibration periods than in the validation periods (Fig. 6).

To compare the results of the flow process simulations with the initial model parameters and the optimized parameters, six evaluation indices (Nash–Sutcliffe coefficient, correlation coefficient, relative flow process error, flood peak error, water balance coefficient, and peak time error) were applied in this study, and the results are presented in Table 3.

Table 3 Flood simulation evaluation indices following parametric optimization.

Table 3 shows that the evaluation indices of the flood simulations after parameter optimization were better than those obtained with the initial model parameters. The average values of the initial parameters for these six indices were 0.81, 0.74, 27%, 31%, 0.80, and 5 h, respectively. For the optimized parameters, the average values were 0.90, 0.91, 16%, 14%, 0.94, and 3 h, respectively. The flood simulation effects after parameter optimization clearly improved, implying that parameter optimization for the QMG model is necessary and that the IPSO algorithm for parameter optimization is an effective approach that can greatly improve the convergence efficiency of parameter optimization and ensure that the model performs well in flood simulations.

4.3 Model validation in flood simulations

Following parameter optimization, we simulated the whole flow process (14 April 2017 to 10 June 2019) based on the optimized and initial parameters of the QMG model (Fig. 6). This approach allowed us to visually assess a long series of flow processes obtained with the model. To reflect the simulation effect of the model for different flood events, we divided the whole flow process into 18 flood events and then used the initial parameters of the model and the optimized parameters to verify the model performance in flood simulations. Figure 7 and Table 4 show the flood simulation effects and the calculated evaluation indices using both the initial and optimized parameters.

Figure 7 Flood simulation effects based on the initial and optimized parameters.

Table 4 Flood simulation indices for model validation.

Figure 7 shows that the flood simulation values obtained using the initial parameters were smaller than the observed values, and the model performance improved in flood simulations after parameter optimization. The simulated flood processes were in good agreement with observations, and flood peak flows were especially well simulated. From the flood simulation indices in Table 4, the average water balance coefficient based on the initial parameters was 0.69, i.e., much less than 1, indicating that the simulated water in the model was unbalanced. After parameter optimization, the average value was 0.92, indicating that parameter optimization had a significant impact on the water balance calculation.

Table 4 shows that the average values of the six indices (Nash–Sutcliffe coefficient, correlation coefficient, relative flow process error, flood peak error, water balance coefficient, and peak time error) for the initial parameters were 0.79, 0.74, 26%, 25%, 0.69, and 5 h, respectively, while for the optimized parameters, the average values were 0.92, 0.90, 10%, 11%, 0.92, and 2 h, respectively. All evaluation indices improved after parameter optimization, with the average values of the Nash coefficient, correlation coefficient, and water balance coefficient increasing by 0.13, 0.16, and 0.23, respectively. Additionally, the average values of the relative flow process error, flood peak error, and peak time error decreased by 15%, 14%, and 3 h, respectively. These reasonable flood simulation results confirmed that parameter optimization with the IPSO algorithm was necessary and effective for the QMG model.

Compared with the overall flow process simulation shown in Figure 6, each flood process was better simulated by the QMG model (Fig. 7). Notably, in the QMG model and the applied algorithm, the main consideration is flood process calculations, and the correlation algorithm for dry-season runoff was not sufficiently described. For example, equations (12)–(15) are used in the flood convergence algorithm. Consequently, the model is not good at simulating other flow processes, such as dry-season runoff, leading to low accuracy in simulations of the overall flow process. The next phase of our research will focus on refining the algorithm related to dry-season runoff and improving the comprehensive performance of the model.

4.4 Uncertainty analysis

4.4.1 Assessment and reduction of uncertainty

In general, the uncertainty in model simulation is due mainly to three factors: (i) the uncertainty of input data, (ii) the uncertainty of the model structure and algorithm and (iii) the uncertainty of the model parameters. In the practical application of a hydrological model, these three uncertainties are usually interwoven, which leads to overall uncertainty in the final simulation results (Krzysztofowicz, 2014). Therefore, this study focused on the uncertainties in the input data, the model structure and the parameters to reduce the overall uncertainty of the simulation results.

First, the input data—mainly rainfall-runoff data and hydrogeological data—were preprocessed, which substantially reduced their uncertainty. Second, we simplified the structure of the QMG model, with only two structural layers in the horizontal and vertical directions. This relatively simple structure greatly reduced the modelling uncertainty. In contrast, our previous Karst–Liuxihe model (Li et al., 2021) included five layers, which led to considerably uncertainty. Third, appropriate algorithms for runoff generation and confluence were selected. In general, different models are designed for different purposes, which leads to notable differences in the algorithms used. In the QMG model, most of the rainfall-runoff algorithms used have been validated by the research results of others, and some of them were improved for karst flood simulation and forecasting with the QMG model. For example, the algorithm for the generation of excess infiltration runoff [Eq. (2)] was an improvement of the version used in the Liuxihe model (Chen, 2009, 2018; Li et al., 2020). Finally, the algorithm for parameter optimization was improved. Considering the shortcomings of the standard PSO algorithm, which tends to converge locally, IPSO for parameter optimization was developed in this study by adding chaotic perturbation factors. The flood simulation results after parameter optimization were much better than those obtained with the initial model parameters (Figs. 6 and 7 and Tables 2 and 3), which indicates that parameter optimization is necessary for distributed hydrological models and can reduce the uncertainty of model parameters.

4.4.2 Sensitivity analysis

The parameter sensitivity results in Table 2 show that the rainfall infiltration coefficient in the QMG model was the most sensitive parameter and was the key to the generation of excess infiltration surface runoff and the separation of surface runoff from subsurface runoff. If the rainfall infiltration coefficient is greater than the infiltration capacity, excess infiltration surface runoff will be generated on exposed karst landforms; otherwise, all rainfall will infiltrate into the vadose zone and then continue to seep into the underground river system, eventually flowing out of the basin through the underground river outlet. The flow modes of surface runoff and underground runoff were completely different, resulting in a large difference in the simulated flow results. Therefore, the rainfall infiltration coefficient had the greatest impact on the final flood simulation results.

Other highly sensitive parameters, such as the rock permeability coefficient, rock porosity and specific yield, were used as the basis for dividing between slow flow in karst fissures and rapid flow in conduits. The division of slow and rapid flows also had a considerable impact on the discharge at the outlet of the basin. Slow flow plays an important role in water storage in karst aquifers and is very important for the replenishment of river base flow in the dry season. Rapid flow in large conduit systems dominates flood runoff and is the main component of the flood water volume in the flood season.

Parameters related to the soil water content, including the saturated water content, field capacity and thickness, were sensitive parameters and had a large influence on the flood simulation results. Notably, the soil moisture content prior to flooding affects how flood flows rise and when peaks occur. If the soil is already very wet or even saturated before flooding, a flood will rise quickly and reach a peak, and the flood peak flow will be sharp and short. This type of flood can easily occur and can lead to a disaster-causing flood event. In contrast, if the soil in the basin is very dry before flooding, the rainfall will first saturate the vadose zone; then, the rainfall will infiltrate into the underground river. The flood peak at the river basin outlet is therefore delayed.

The moderately sensitive parameters were the flow direction, slope and soil coefficient; they had a specific influence on the flood simulation results, but the influence was not as great as that of the highly sensitive and sensitive parameters. The insensitive parameters were channel roughness and the evaporation coefficient. The amount of water lost via evapotranspiration is very small compared to the total volume of flood water, and evapotranspiration was therefore the least-sensitive parameter in the QMG model.

5 Conclusions

In this study, a new distributed physically based hydrological model, i.e., the QMG model, was proposed to accurately simulate floods in karst trough and valley landforms. The main conclusions of this paper are as follows.

The QMG model has high application potential in karst hydrology simulations. Other distributed hydrological models usually have multiple structures, resulting in the need for a large amount of data to build models in karst areas (Kraller et al., 2014). The QMG model has only a double-layer structure, with clear physical meaning, and a small amount of basic data, such as some necessary hydrogeological data, is needed to build the model in karst areas. For example, the distribution and flow direction of underground rivers must be known and can be inferred from tracer tests at low cost. There are fewer parameters in the QMG model than in other distributed hydrological models, with only 10 parameters that need to be calibrated.

The flood simulations after parameter optimization were much better than those based on the initial model parameters. After parameter optimization, the average values of the Nash coefficient, correlation coefficient and water balance coefficient increased by 0.13, 0.16 and 0.23, respectively, and the average relative flow process error, flood peak error and peak time error decreased by 15%, 14% and 3 h, respectively. Parameter optimization is necessary for distributed hydrological models, and the improved IPSO algorithm in this study was effective.

In the QMG model, the rainfall infiltration coefficient I_c, the rock permeability coefficient K, the rock porosity R_p and the parameters related to the soil water content were sensitive parameters. The order of parameter sensitivity was infiltration coefficient > permeability coefficient > rock porosity > specific yield > saturated water content > field capacity > flow direction > thickness > slope > soil coefficient > channel roughness > evaporation coefficient.

This QMG model is suitable for karst trough and valley landforms, such as those in the study area, where the topography is conducive to the spread of flood water. In the future, it must be verified whether this model is applicable to other karst areas and landforms. In addition, although the studied basin area is very small, but the hydrological similarity among different small basin areas varies greatly (Kong and Rui, 2003). The size of the area to be modelled has a great influence on the choice of spatial resolution for modelling (Chen et al., 2017). Therefore, it must be determined whether the QMG model is suitable for flood forecasting in large karst basins.

Model development.

The QMG model presented in this study uses Visual Basic language programming. The general framework of the model and the algorithm consist of three parts: the modelling approach, the rainfall-runoff generation and convergence algorithm, and the parameter optimization algorithm. As a free and open-source hydrological modelling program (QMG model-V1.0), we provide all modelling packages, including the model code, installation package, simulation data package and user manual, free of charge. It is important to note that the model we provide is for scientific research purposes only and should not be used for any commercial purposes (Creative Commons Attribution 4.0 International).

The model installation program can be downloaded from Zenodo and should be cited as (JI LI. (2021, June 16). QMG model-V1.0. Zenodo. http://doi.org/10.5281/zenodo.4964701 and http://doi.org/10.5281/zenodo.4964697) (registration required). The user manual can be downloaded from http://doi.org/10.5281/zenodo.4964754.

Code availability.

All codes for the QMG model-V1.0 in this paper are available and free, and the code can be downloaded from Zenodo at http://doi.org/10.5281/zenodo.4964709 (registration required) (Cite as JI LI. (2021, June 16). QMG model-V1.0 code (Version v1.0). Zenodo).

Data availability.

All data used in this paper are available, findable, accessible, interoperable, and reusable.

The simulation data and modelling data package can be downloaded from http://doi.org/10.5281/zenodo.4964727. The DEM was downloaded from the Shuttle Radar Topography Mission database at http://srtm.csi.cgiar.org. The land use-type data were downloaded from http://landcover.usgs.gov, and the soil-type data were downloaded from http://www.isric.org. These data were last accessed on 15 October 2020.

Author contributions. JIL was responsible for the calculations and writing of the whole paper. DY helped conceive the structure of the model. ZF and JL provided significant assistance in the English translation of the paper. MM provided flow data from the study area.

Competing interests.

The authors declare that they have no conflicts of interest.

Acknowledgements.

This study was supported by the National Natural Science Foundation of China (41830648), the National Science Foundation for Young Scientists of China (42101031), the Fundamental Research Funds for the Central Universities (), Chongqing Natural Science Foundation (cstc2021jcyj-msxm0007), and the Chongqing Education Commission Science and Technology Research Foundation (KJQN202100201), the Drought Monitoring, Analysis and Early Warning Project for Typical Drought-Prone Areas in Chongqing (20C00183) and the Open Project Program of the Guangxi Key Science and Technology Innovation Base on Karst Dynamics (KDL & Guangxi 202009, KDL & Guangxi 202012).

References

Abbott, M. B., Bathurst, J. C., Cunge, J. A., O'Connell, P. E., and Rasmussen, J.: An Introduction to the European HydrologicSystem-System Hydrologue Europeen, 'SHE', a: History and Philosophy of a Physically-based, Distributed Modelling System,J. Hydrol., 87, 45–59, 1986a.

Abbott, M. B., Bathurst, J. C., Cunge, J. A., O'Connell, P. E., and Rasmussen, J.: An Introduction to the European Hydrologic System-System Hydrologue Europeen, 'SHE', b: Structure of a Physically based, distributed modeling System, J. Hydrol., 87,61–77, 1986b.

Ambroise, B., Beven, K., and Freer, J.: Toward a generalization of the TOPMODEL concepts: Topographic indices of hydrologic similarity. Water Resources Research, 32, 2135-2145, 1996.

Atkinson, T.C.: Diffuse flow and conduit flow in limestone terrain in the Mendip Hills, Somerset (Great Britain). Journal of Hydrology, 35, 93-110. https://doi.org/10.1016/0022-1694(77)90079-8, 1977.

Berry, R.A., Saurel, R., and Lemetayer, O.: The discrete equation method (DEM) for fully compressible, two-phase flows in ducts of spatially varying cross-section. Nuclear Engineering & Design, 240(11), 3797-3818, 2010.

Beven, K., and Binley, A.: The future of distributed models: Model calibration and uncertainty prediction. Hydrological Processes, 6, 279-298, 2006.

Birk, S., Geyer, T., Liedl, R., and Sauter, M.: Process-based interpretation of tracer tests in carbonate aquifers. Ground Water, 43(3), 381-388, 2005.

Bittner, D., Parente, M.T., Mattis, S., Wohlmuth, B., and Chiogna, G.: Identifying relevant hydrological and catchment properties in active subspaces: An inference study of a lumped karst aquifer model. ADVANCES IN WATER RESOURCES,135,550-560. doi: 10.1016/j.advwatres.2019.103472, 2020.

Blansett, K. L., and Hamlett, J. M.: Challenges of Stormwater Modeling for Urbanized Karst Basins. Pittsburgh, Pennsylvania, an ASABE Meeting Presentation, Paper Number: 1009274. doi:10.13031/2013.29840, 2010.

Blansett, K. L.: Flow, water quality, and SWMM model analysis for five urban karst basins.. (Doctoral dissertation). The Pennsylvania State University,USA, 2011.

Bonacci, O., Ljubenkov, I., and Roje-Bonacci, T.: Karst flash floods: an example from the Dinaric karst Croatia. Nat. Hazards Earth Syst. Sci. 6, 195–203, 2006.

Chang, Y., and Liu, L.: A review of hydrological models in karst areas. Engineering investigation, 43,37-44, 2015.

Chen, G.M., Jia, J.Y., and Han, Q.: Research on inertia weight reduction strategy of Particle Swarm optimization algorithm. Journal of Xi'an Jiaotong University, 40(1),53-56, 2006.

Choi, J., Harvey, J. W., and Conklin, M. H.: Use of multi-parameter sensitivity analysis to determine relative importance of factors influencing natural attenuation of mining contaminants. the Toxic Substances Hydrology Program Meeting, Charleston,South Carolina, 1999.

Chen, Y. B.: Liuxihe Model, China Science and Technology Press, Beijing, China, 2009.

Chen, Y., Li, J., and Xu, H.: Improving flood forecasting capability of physically based distributed hydrological models by parameter optimization. Hydrol. Earth Syst. Sci. 20, 375-392. https://doi.org/10.5194/hess-20-375-2016, 2016.

Chen, Y., Li, J., Wang, H., Qin, J., and Dong, L.: Large watershed flood forecasting with high-resolution distributed hydrological model. Hydrol. Earth Syst. Sci. 21, 735-749. https://doi.org/10.5194/hess-21-735-2017, 2017.

Chen, Y.: Distributed Hydrological Models. Springer Berlin Heidelberg, Berlin, Germany. https://doi.org/10.1007/978-3-642-40457-3_23-1, 2018.

Dewandel, B., Lachassagne, P., Bakalowicz, M., Weng, P., and Malki, A.A.: Evaluation of aquifer thickness by analysing recession hydrographs. Application to the Oman ophiolite hard-rock aquifer. Journal of Hydrology, 274,248-269, 2003.

Dubois, E., Doummar, J., Séverin Pistre, S., and Larocque, M.: Calibration of a lumped karst system model and application to the Qachqouch karst spring (Lebanon) under climate change conditions. Hydrol. Earth Syst. Sci., 24, 4275-4290. https://doi.org/10.5194/hess-24-4275-2020, 2020.

Doummar, J., Sauter, M., and Geyer, T.: Simulation of flow processes in a large scale karst system with an integrated catchment model (MIKE SHE) – identification of relevant parameters influencing spring discharge. Journal of Hydrology, 426-427, 112-123, 2012.

Epting, J., Page, R.M., and Auckenthaler, A.: Process-based monitoring and modeling of Karst springs–Linking intrinsic to specific vulnerability. Science of the Total Environment, 625, 403-415, 2018.

Fleury, P., Plagnes, V., and Bakalowicz, M.: Modelling of the functioning of karst aquifers with a reservoir model: Application to Fontaine de Vaucluse (South of France). Journal of Hydrology, 345,38-49. http://dx.doi.org/10.1016/j.jhydrol.2007.07.014, 2007b.

Ford, D. C., and Williams, P.W.: Karst geomorphology and hydrology. Wiley, Chichester, England, 2007.

Gang, L., Tong, F.G., and Bin,T.: A Finite Element Model for Simulating Surface Runoff and Unsaturated Seepage Flow in the Shallow Subsurface. Hydrological Processes, 6,102-120. doi: 10.1002/hyp.13564, 2019.

Geyer, T., Birk, S., Liedl, R., and Sauter, M.: Quantification of temporal distribution of recharge in karst systems from spring hydrographs. Journal of Hydrology, 348(30), 452-463, 2008.

Gou, P.F., Jiang, Y.J., Hu, Z.Y., Pu, J.B., and Yang, P.H.: A study of the variations in hydrology and hydrochemistry under the condition of a storm in a typical karst subterranean stream. HYDROGEOLOGY&ENGINEERING GEOLOGY,37(5),20-25, 2010.

Gutierrez, F.: Hazards associated with karst. In: Alcantara, I. & A. Goudie (Eds.), Geomorphological Hazards and Disaster Prevention. Cambridge University Press, Cambridge, 161–175, 2010.

Gutierrez, F., Parise, M., D' Waele, J., and Jourde, H.: A review on natural and human-induced geohazards and impacts in karst. Earth Science Reviews, 138, 61-88, 2014.

Hartmann, A., and Baker, A.: Progress in the hydrologic simulation of time variant of karst systems-Exemplified at a karst spring in Southern Spain. Advances in Water Resources, 54,149-160, 2013.

Hartmann, A., Goldscheider, N., Wagener, T., Lange, J., and Weiler, M.: Karst water resources in a changing world: Review of hydrological modeling approaches. Reviews of Geophysics 52: 218-242. doi: 10.1002/2013RG000443, 2014a.

Hartmann, A., and Baker, A.: Modelling karst vadose zone hydrology and its relevance for paleoclimate reconstruction. Earth-Science Reviews, 172, 178-192, 2017.

Hartmann, A.: Experiences in calibrating and evaluating lumped karst hydrological models. London: Geological Society, Special Publications, 2018.

Jourde, H., Roesch, A., Guinot, V., and Bailly-Comte, V.: Dynamics and contribution of karst groundwater to surface flow during Mediterranean flood. Environ. Geol. 51 (5), 725–730, 2007.

Jourde, H., Lafare, A., Mazzilli, N., Belaud, G., Neppel, L., Doerfliger, N., and Cernesson, F.: Flash flood mitigation as a positive consequence of anthropogenic forcings on the groundwater resource in a karst catchment. Environ. Earth Sci. 71, 573–583,2014.

Jukić, D., and Denić-Jukić, V.: Groundwater balance estimation in karst by using a conceptual rainfall–runoff model. Journal of Hydrology, 373, 302-315. http://dx.doi.org/10.1016/j.jhydrol.2009.04.035, 2009.

Kong, F.Z., and Rui, X.F.: Hydrological similarity of catchments based on topography.

GEOGRAPHICAL RESEARCH, (06), 709-715, 2003.

Kovács, A., and Sauter, M.: Modelling karst hydrodynamics. In: Goldscheider N, Drew D (eds) Methods in karst hydrogeology, IAH international contributions to hydrogeology; 26,264 p, 2007.

Kovács, A., and Perrochet, P.: A quantitative approach to spring hydrograph decomposition. Journal of Hydrology, 352, 16-29. http://dx.doi.org/10.1016/j.jhydrol.2007.12.009, 2008.

Kurtulus, B., and Razack, M.: Evaluation of the ability of an artificial neural network model to simulate the input-output responses of a large karstic aquifer: the la rochefoucauld aquifer (charente, france). Hydrogeology Journal, 15(2), 241-254, 2007.

Krzysztofowicz, R., and Kelly, K.: Hydrologic uncertainty processor for probabilistic river stage forecasting. Water Resources Research, 36(11),3265-3277, 2000.

Krzysztofowicz, R.: Probabilistic flood forecast： Exact and approximate predictive distributions. Journal of Hydrology, 517(1), 643-651, 2014.

Kraller, G., Warscher, M., Strasser, U., Kunstmann, H., and Franz, H.: Distributed hydrological modeling and model adaption in high alpine karst at regional scale (berchtesgaden alps, germany). Springer International Publishing Switzerland. https://doi.org/10.1007/978-3-319-06139-9_8, 2014.

Ladouche, B., Marechal, J. C., and Dorfliger, N.: Semi-distributed lumped model of a karst system under active management. Journal of Hydrology, 509,215-230, 2014.

Li, J., Chen, Y., Wang, H., Qin, J., Li, J., and Chiao, S.: Extending flood forecasting lead time in a large basin by coupling WRF QPF with a distributed hydrological model, Hydrol. Earth Syst. Sci. 21, 1279–1294. https://doi.org/10.5194/hess-21-1279-2017, 2017.

Li, J., Yuan, D., Liu, J., Jiang, Y., Chen, Y., Hsu, K. L., and Sorooshian, S.: Predicting floods in a large karst river basin by coupling PERSIANN-CCS QPEs with a physically based distributed hydrological model. Hydrol. Earth Syst. Sci. 23, 1505-1532.

https://doi.org/10.5194/hess-23-1505-2019, 2019.

Li, J., Hong, A., Yuan, D., Jiang,Y., Deng,S., Cao,C., and Liu, J.: A new distributed karst-tunnel hydrological model and tunnel hydrological effect simulations. Journal of Hydrology, 593, 125639. https://doi.org/10.1016/j.jhydrol.2020.125639, 2020.

Li, J., Hong, A., Yuan, D., Jiang,Y., Zhang,Y., Deng,S., Cao,C., Liu, J., and Chen,Y.: Elaborate Simulations and Forecasting of the Effects of Urbanization on Karst Flood Events Using the Improved Karst-Liuxihe Model.CATENA,197,104990. https://doi.org/10.1016/j.catena.2020.104990, 2021.

Li, J., Yuan, D., Ma, M., and Liu, J.: Simulation of Karst Floods with a Hydrological Model Improved by Meteorological Model Coupling, Journal of Hydrometeorology, 23(2),185-207. doi: 10.1175/JHM-D-21-0088.1, 2022.

Liedl, R.., Sauter, M., Huckinghaus, D., Clemens, T., and Teutsch, G.: Simulation of the development of karst aquifers using a coupled continuum pipe flow model. Water Resources Research, 39, 50-57, 2003.

Liu, X., Jiang, Y.J., Ye, M.Y., Yang, P.H., Hu, Z.Y., and Li, Y.Q.: Study on hydrologic regime of underground river in typical karst valley- A case study on the Qingmuguan subterranean stream in Chongqing. CARSOLOGICA SINICA, 28(2),149-154, 2009.

Lu, D. B., Shi, Z. T., Gu, S. X., and Zeng, J. J.: Application of Hydrological Model in the Karst Area. Water-saving irrigation.11, 31-34. doi:1007-4929(2013)11-031-04, 2013.

Martinotti, M.E., Pisano, L., Marchesini, I., Rossi, M., Peruccacci, S., Brunetti, M.T., Melillo, M.,Amoruso, G., Loiacono, P., Vennari, C., Vessia, G., Trabace, M., Parise, M., and Guzzetti, F.: Landslides, floods and sinkholes in a karst environment: the 1–6 September 2014 Gargano event, southern Italy. Natural Hazards and Earth System Sciences, 17, 467-480, 2017.

Meng, H.H., Wang, N.C., Su, W.C., and Huo, Y.: Modeling and application of karst semi-distributed hydrological model based on sinkholes. SCIENTIA GEOGRAPHICA SINICA, 5, 550-554. doi: 10.3969/j.issn.1000-0690.2009.04.014, 2009.

Meng, H.H., and Wang, N.C.: Advances in the study of hydrological models in karst basin. Progress in Geography, 29,1311-1318, 2010.

Pan, H.Y.: Hydrological model and application in karst watersheds. China University of Geosciences. Doctoral Dissertation, Wuhan, China, 2014.

Parise, M.: Hazards in karst, Proceedings Int. Conf. "Sustainability of the karst environment. Dinaric karst and other karst regions", IHP-Unesco, Series on Groundwater,2, 155-162, 2010.

Peterson, E.W., and Wicks, C. M.: Assessing the importance of conduit geometry and physical parameters in karst systems using the storm water management model (SWMM).Journal of Hydrology, 329, 1-2, 294-305, 2006.

Peterson, J.R., and Hamlett, J.M.: Hydrologic calibration of the SWAT model in a basin containing fragipan soils. JAWRA Journal of the American Water Resources Association. doi: 10.1111/j.1752-1688.1998. tb00952.x, 1998.

Petrie, R., Denvil, S., Ames, S.,et al.: Coordinating an operational data distribution network for CMIP6 data, Geosci. Model Dev., 14, 629–644.

https://doi.org/10.5194/gmd-14-629-2021, 2021.

Qin, J.G., and Jiang, Y.P.: A review of numerical simulation methods for CFP pipeline flow. Groundwater. 3, 98-100, 2014.

Reimann, T., Melissa, E., and Hill.: Modflow-cfp: a new conduit flow process for modflow–2005. Ground Water,47(3),321-325. doi:10.1111/j.1745-6584.2009.00561.x, 2009.

Ren, Q.W.: Water Quantity Evaluation Methodology Based on Modified SWAT Hydrological Modeling in Southwest Karst Area, China University of Geoscience, Wuhan, China, 2006.

Shoemaker, W.B., Cunningham, K.J., and Kuniansky, E.L.: Effects of turbulence on hydraulic heads and parameter sensitivities in preferential groundwater flow layers.

Water Resources Research, 44, 34-50. doi: 10.1029/2007WR006601, 2008.

Suo, L.T., Wan, J.W., and Lu, X.W.: Improvement and application of TOPMODEL in karst region. Carsologica Sinica, 26(1), 67-70, 2007.

Teixeiraparente, M., Bittner, D., Mattis, S.A., Chiogna, G , and Wohlmuth, B.: Bayesian calibration and sensitivity analysis for a karst aquifer model using active subspaces. Water Resources Research, 55, 342-356. doi: 10.1029/2019WR024739, 2019.

White, W.B.: Karst hydrology: recent developments and open questions. Eng. Geol. 65, 85–105, 2002.

Williams, P.W.: The role of the epikarst in karst and cave hydrogeology: a review. Int. J. Speleol. 37, 1–10, 2008.

Williams, P. W.: Book Review: Methods in Karst Hydrogeology, Nico Goldscheider and David Drew (eds). Hydrogeology Journal, 17,1025-1025, 2009.

Worthington, S., Ford, D., and Beddows, P.: Porosity and permeability enhancement in unconfined carbonate aquifers as a result of solution. Speleogenesis: evolution of karst aquifers, 2000.

Yang, P. H., Luo, J.Y., Peng, W., Xia, K.S., and Lin, Y.S.: Application of online technique in tracer test-A case in Qingmuguan subterranean river system, Chongqing, China. CARSOLOGICA SINICA, 27(3),215-220, 2008.

Yu, D., Yin, J., Wilby, R.L., Stuart, N. L., Jeroen, C., Lin, N., Liu, M., Yuan, H., Chen, J., Christel, P., Guan, M., Avinoam, B., Charlie, W. D., Tang, X., Yu, L., and Xu, S.: Disruption of emergency response to vulnerable populations during floods. Nature Sustainability, 3, 728–736. https://doi.org/10.1038/s41893-020-0516-7, 2020.

Yu, Q., Yang, P.H., Yu, Z.L., Chen, X.B., and Wu, H.: Dominant factors controlling hydrochemical variationg of karst underground river in different period, Qingmuguan,Chongqing. CARSOLOGICA SINICA, 35(2),134-143, 2016.

Zhang, Q.: Assesment on the intrinsic vulnerability of karst groundwater source in the Qingmuguan karst valley. CARSOLOGICA SINICA, 31(1),67-73, 2012.

Zhu, C., and Li, Y.：Long-Term Hydrological Impacts of Land Use/Land Cover Change From 1984 to 2010 in the Little River Basin, Tennessee. International Soil and Water Conservation Research, 2(2), 11-21, 2014.

Tables

Table 1 Parameters of the QMG model.

Parameters	Variable name	Physical property
Infiltration coefficient	I_c	Meteorological
Evaporation coefficient	λ	Vegetation cover
Soil thickness	h	Karst aquifer
Soil coefficient	S_b	Soil type
Saturated water content	S_c	Soil type
Rock porosity	R_p	Karst aquifer
Field capacity	F_c	Soil type
Permeability coefficient	K	Karst aquifer
Flow direction	F_d	Landform
Slope	S_0	Landform
Specific yield	S_y	Karst aquifer
Channel roughness	n	Landform

Table 2 Parametric sensitivity results in the QMG model.

I_c	λ	h	S_b	S_c	S_y	F_d	S_0	R_p	F_c	K	n
0.92	0.24	0.71	0.58	0.8	0.83	0.74	0.68	0.86	0.78	0.89	0.36

Table 3 Flood simulation evaluation index through parametric optimization.

Parameter optimization	Parameter types	Nash coefficient	Correlation coefficient	Relative flow process error/%	Flood peak error/%	Water balance coefficient	Peak time error (hours)
Calibration periods	Initial	0.82	0.77	24	29	0.82	4
	Optimized	0.91	0.94	14	12	0.95	2
Validation periods	Initial	0.79	0.71	29	32	0.77	6
	Optimized	0.88	0.87	18	16	0.92	3
Average value	Initial	0.81	0.74	27	31	0.8	5
	Optimized	0.9	0.91	16	14	0.94	3

Table 4 Flood simulation indices for model validation.

Floods	Parameter types	Nash coefficient	Correlation coefficient	Relative flow process error/%	Flood peak error/%	Water balance coefficient	Peak time error/(hours)
2017042408	Initial	0.77	0.7	28	29	0.71	-5
	Optimized	0.95	0.89	11	15	0.88	-2
2017050816	Initial	0.78	0.71	19	19	0.76	-4
	Optimized	0.92	0.88	11	9	0.94	-2
2017061518	Initial	0.76	0.6	25	32	0.63	-5

	Optimized	0.91	0.93	12	11	0.95	-3
2017071015	Initial	0.78	0.82	25	37	0.64	-4
	Optimized	0.92	0.87	8	7	0.94	-2
2017091512	Initial	0.81	0.62	21	16	0.78	-5
	Optimized	0.9	0.92	13	10	0.9	-4
2017100815	Initial	0.75	0.68	30	26	0.62	-2
	Optimized	0.94	0.86	11	15	0.92	-1
2018052016	Initial	0.78	0.68	25	21	0.67	5
	Optimized	0.91	0.93	10	13	0.94	2
2018060815	Initial	0.82	0.79	27	22	0.69	-6
	Optimized	0.9	0.92	11	12	0.93	-4
2018071212	Initial	0.84	0.75	26	24	0.61	5
	Optimized	0.91	0.88	8	15	0.92	3
2018081512	Initial	0.71	0.78	26	24	0.78	-4
	Optimized	0.89	0.94	12	11	0.89	-3
2018090516	Initial	0.85	0.68	28	23	0.68	-5
	Optimized	0.93	0.87	12	10	0.92	-2
2018092514	Initial	0.79	0.78	23	19	0.59	5
	Optimized	0.88	0.88	9	11	0.89	2
2018101208	Initial	0.78	0.81	28	25	0.63	5
	Optimized	0.92	0.94	11	10	0.94	2
2018111208	Initial	0.79	0.81	25	24	0.65	-6
	Optimized	0.94	0.86	13	12	0.92	-2
2019042512	Initial	0.78	0.8	26	36	0.8	5
	Optimized	0.89	0.94	9	16	0.93	2
2019051513	Initial	0.84	0.77	32	27	0.79	4
	Optimized	0.91	0.88	9	13	0.95	2
2019052516	Initial	0.74	0.75	29	26	0.63	-5
	Optimized	0.92	0.86	7	15	0.96	-2
2019060518	Initial	0.85	0.83	28	25	0.78	-4
	Optimized	0.95	0.96	10	12	0.92	-2
Average value	Initial	0.79	0.74	26	25	0.69	5
	Optimized	0.92	0.9	10	11	0.92	2

Figures

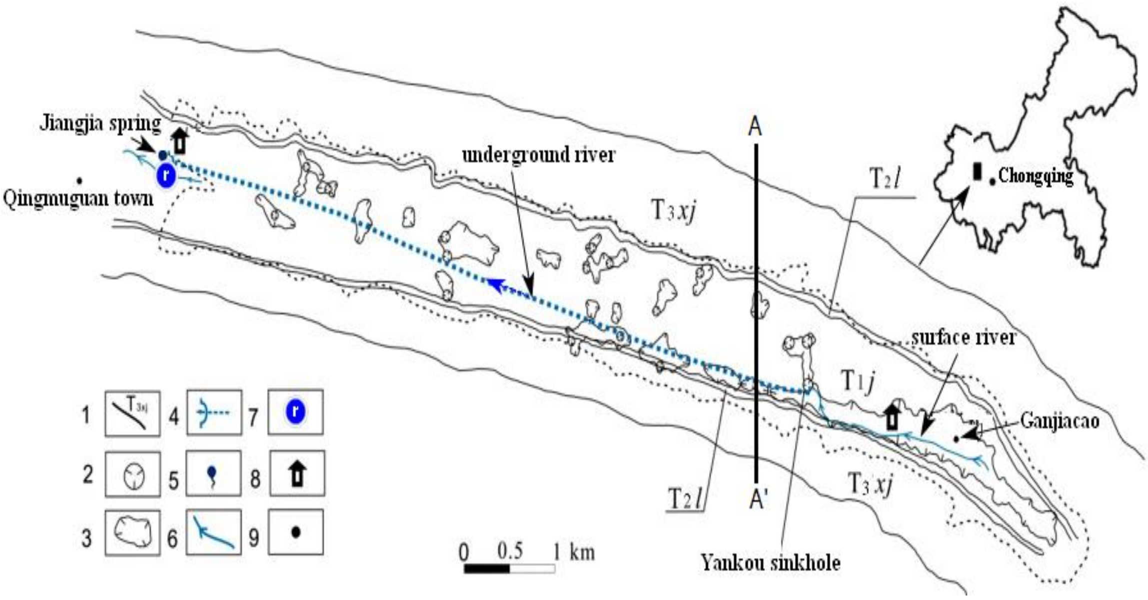

1- stratigraphic boundary, 2- sinkhole, 3- karst depression, 4- underground river, 5- karst spring, 6- surface river, 7- river gauge, 8- rain gauge, and 9- geographical name

a. Qingmuguan karst basin (modified from Yu et al., 2016)

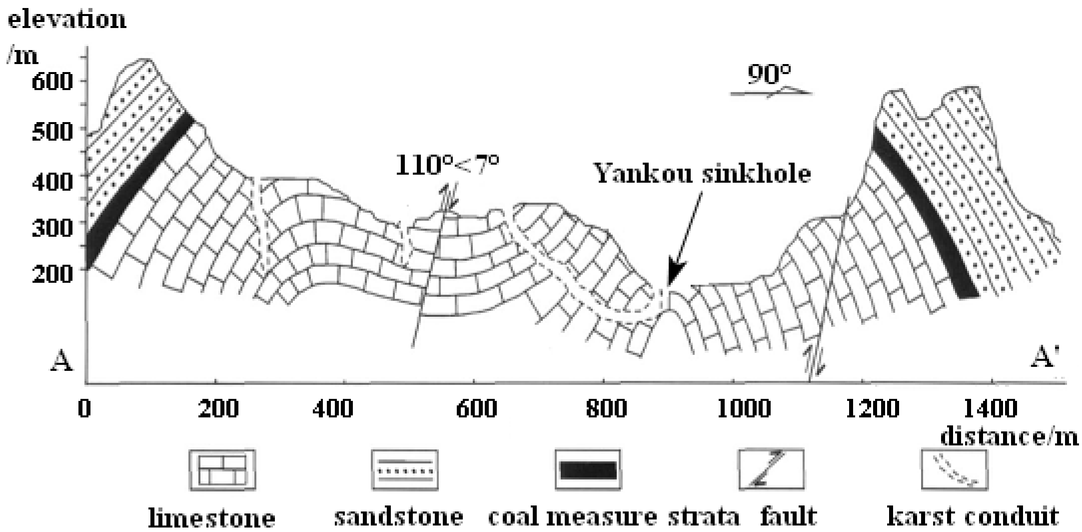

b. Lithologic cross section AA' of the Yankou sinkhole (modified from Zhang, 2012)

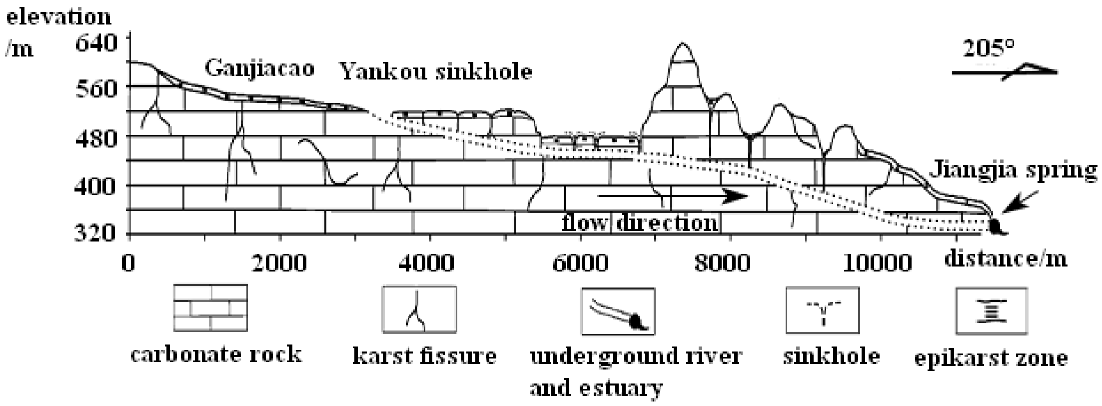

c. Longitudinal profile of the study area (modified from Yang et al.,2008)

Figure 1 The Qingmuguan karst basin.

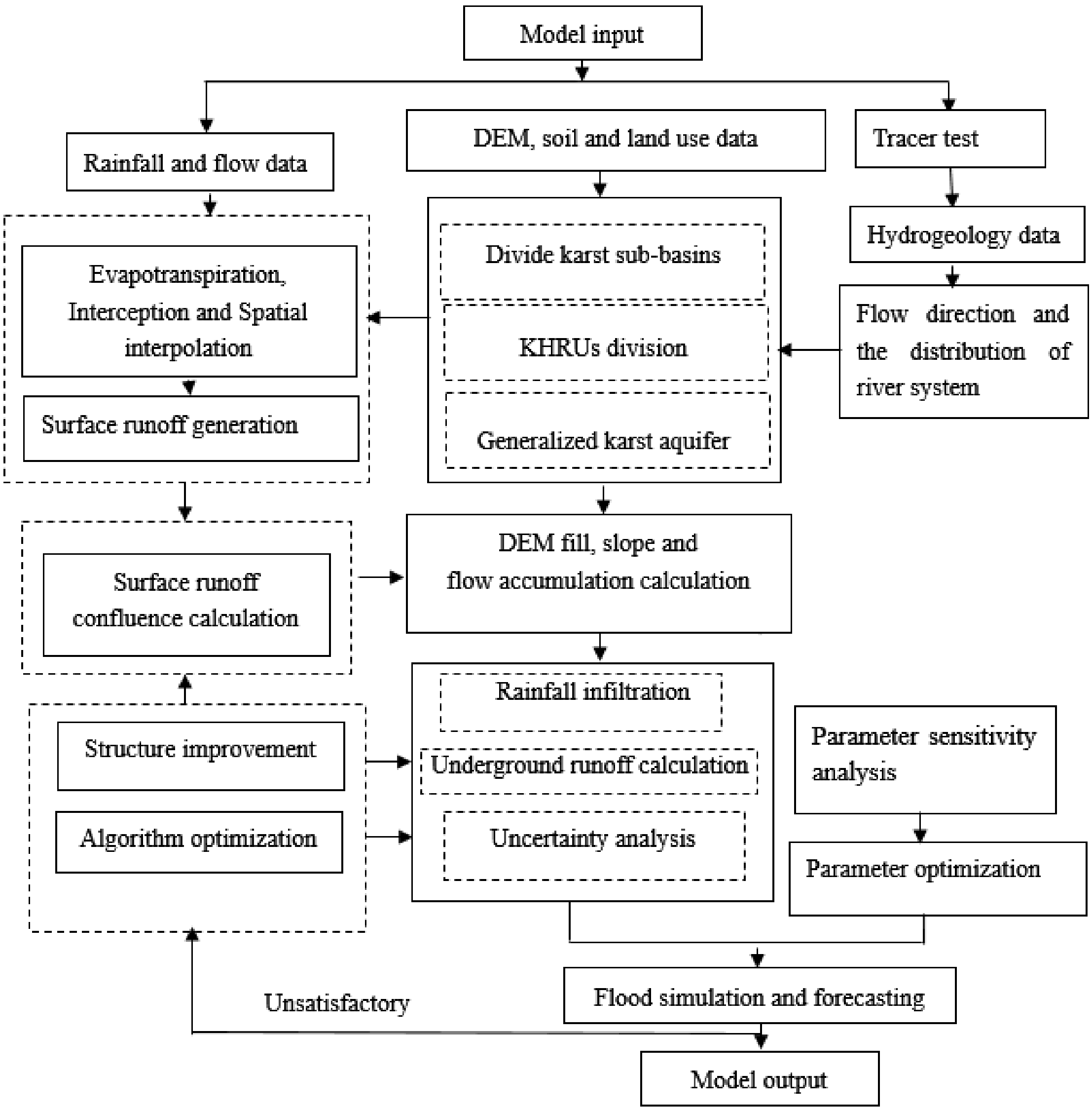

Figure 2 Modelling flowchart of the QMG (Qingmuguan) model.

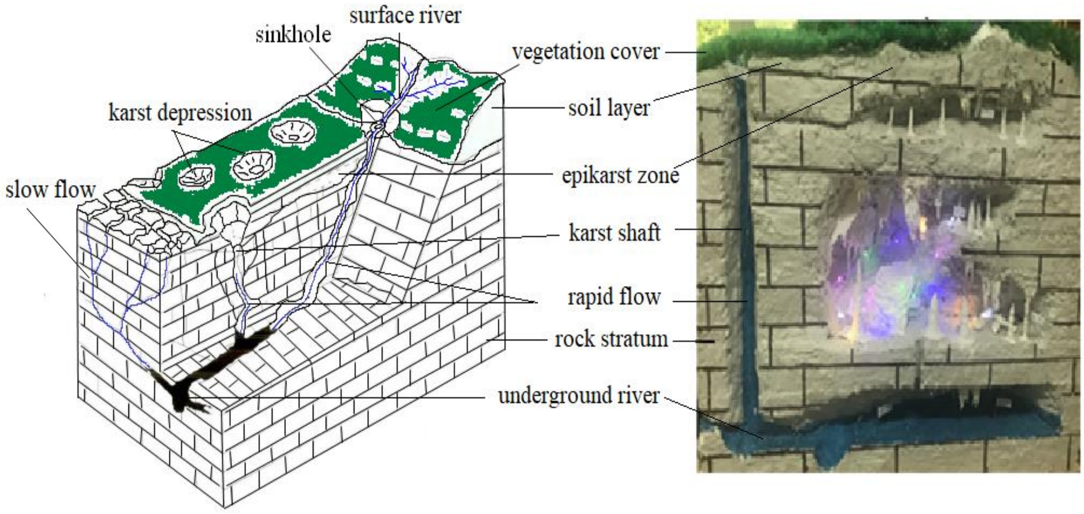

Figure 3 Spatial structure of the KHRUs (Li et al., 2021).

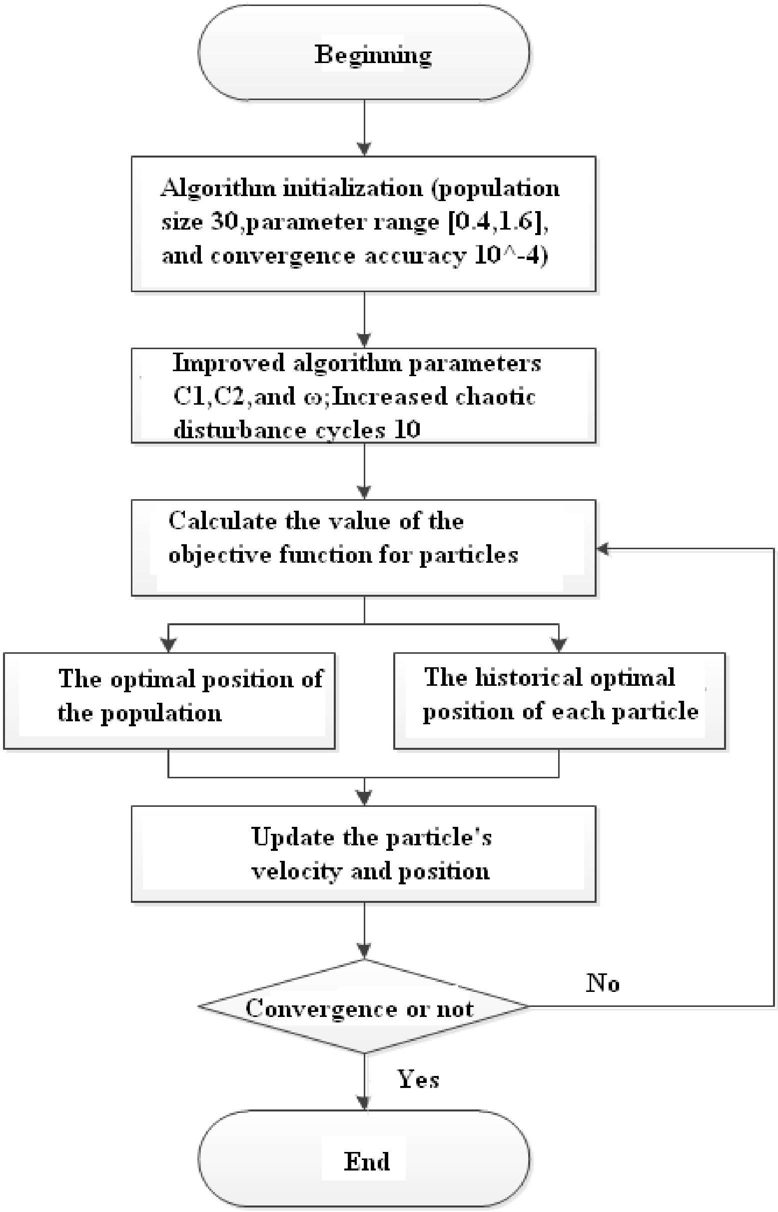

Figure 4 Algorithm flowchart of IPSO.

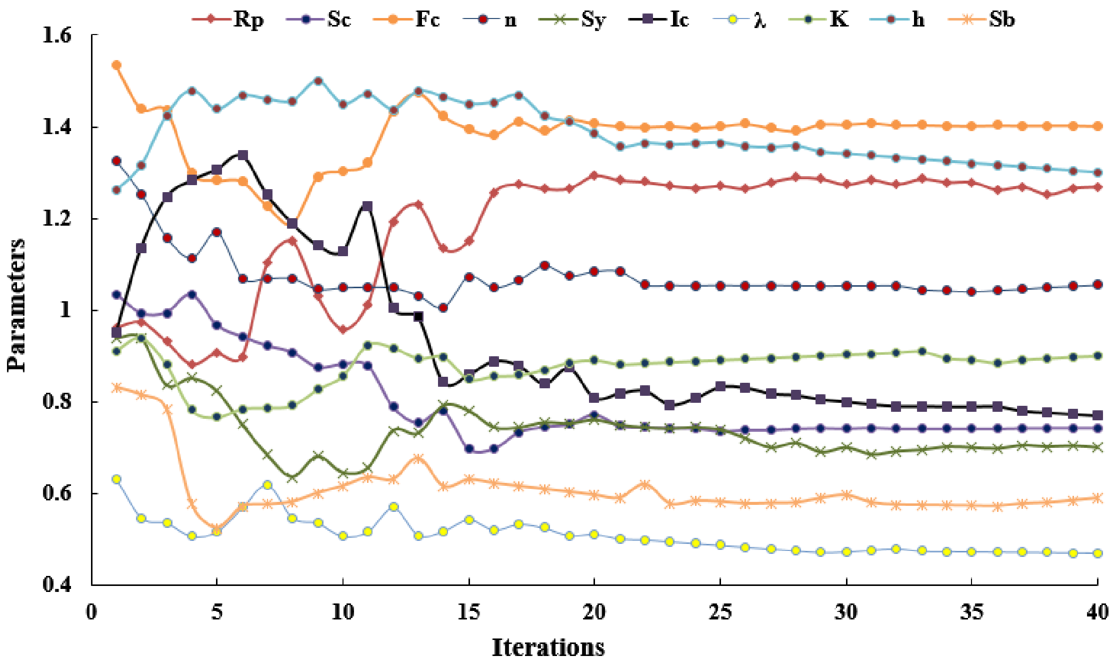

Figure 5 Iterative process of parameter optimization.

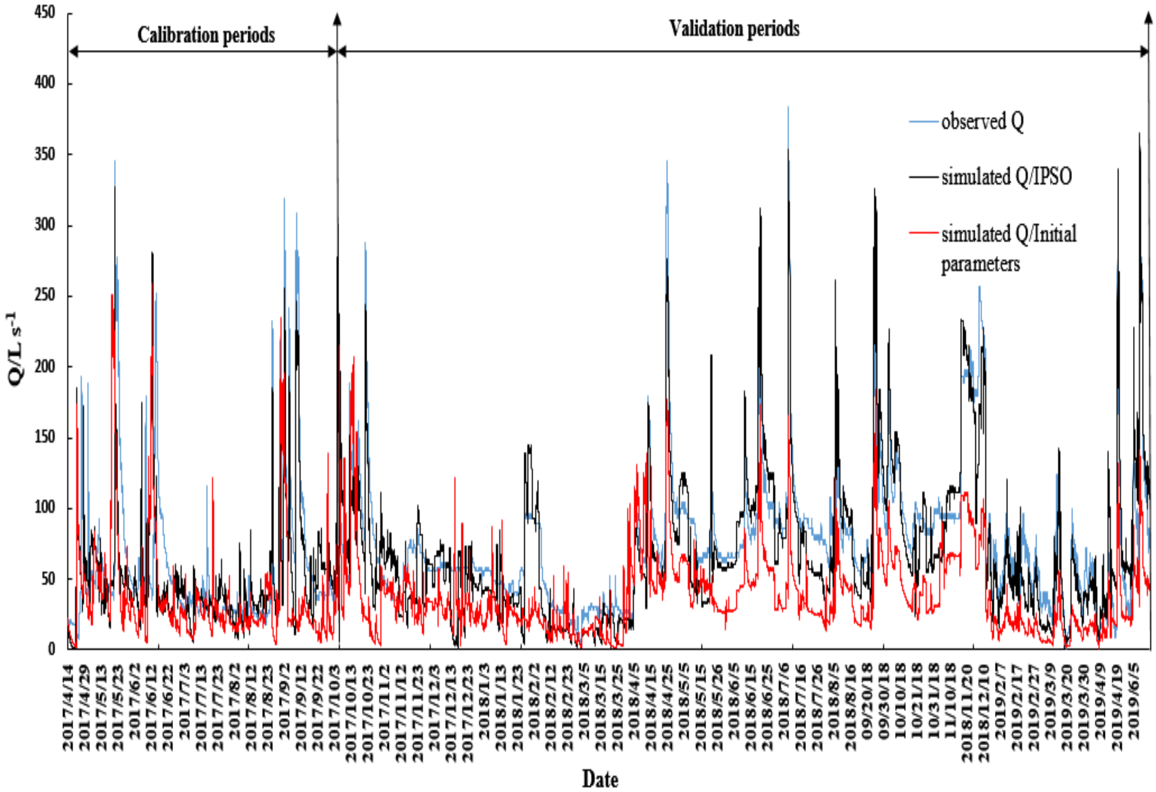

Figure 6 Flow simulation results of the QMG model based on parameter optimization.

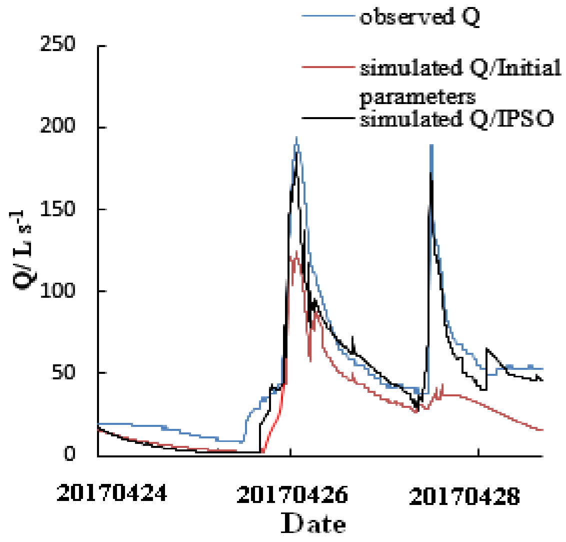

a. flood 201704240800

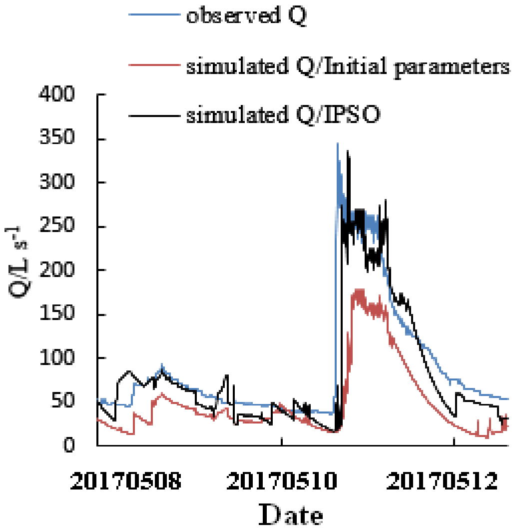

b. flood 201705081600

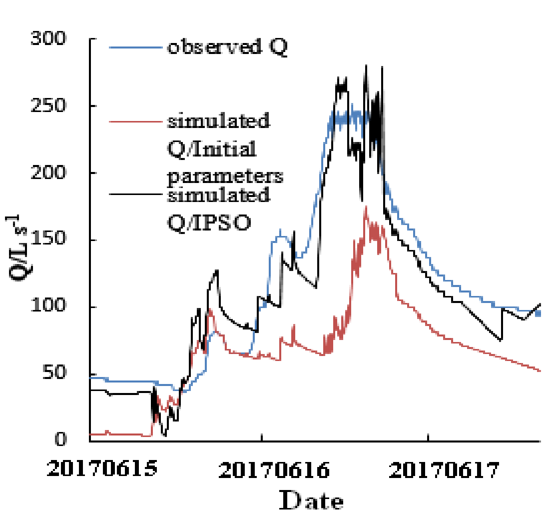

c. flood 201706151800

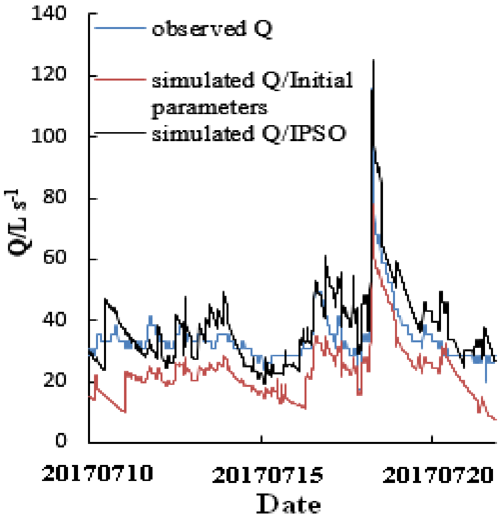

d. flood 201707101530

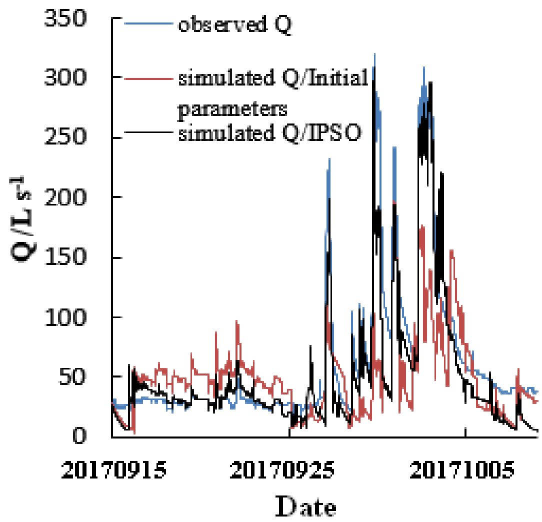

e. flood 201709151200

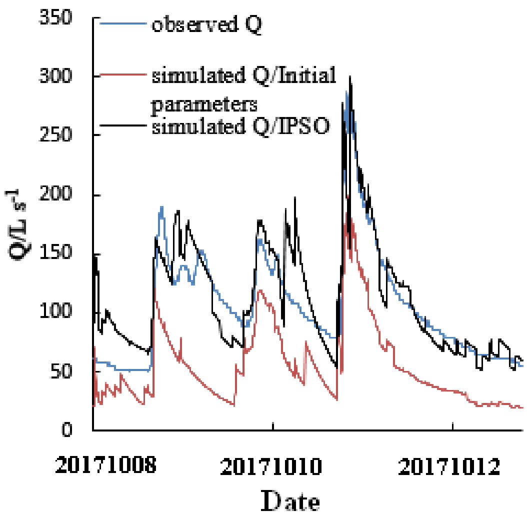

f. flood 201710081500

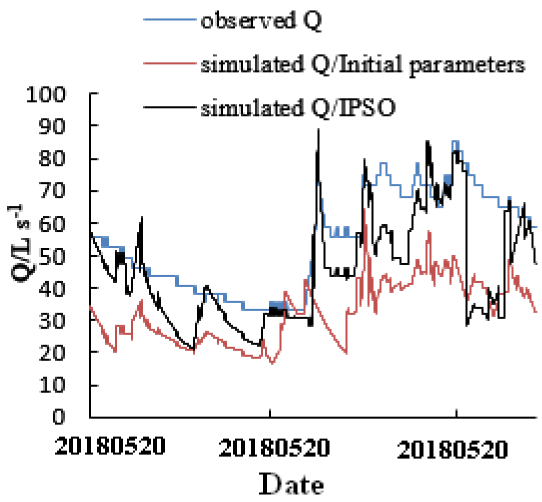

g. flood 201805201600

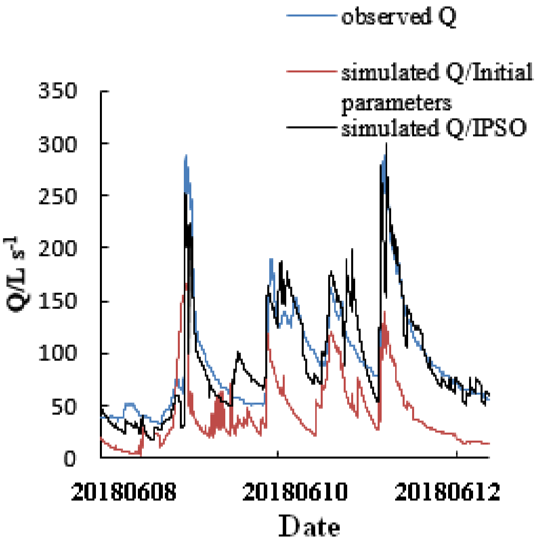

h. flood 201806081500

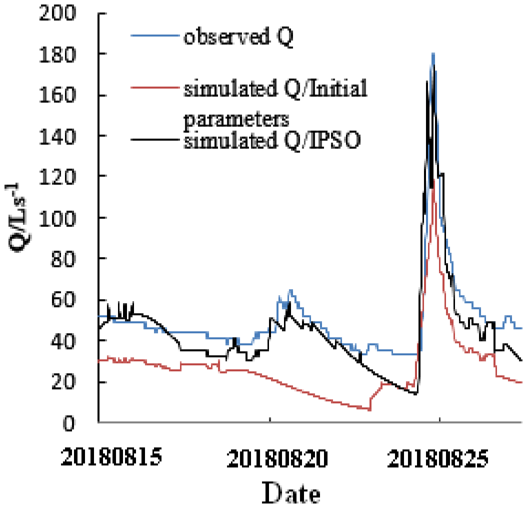

i. flood 201808151200

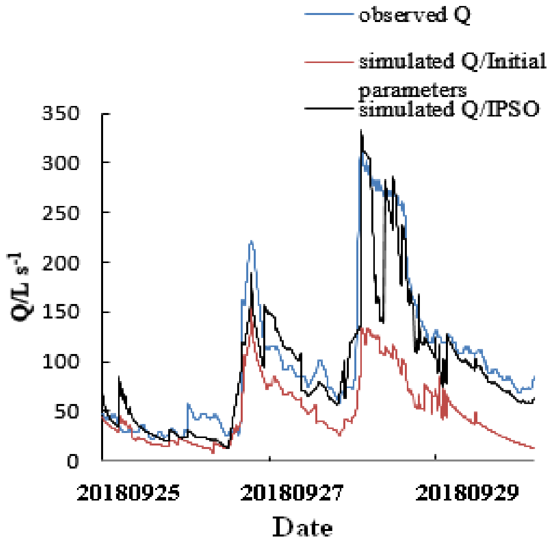

j. flood 201905251600

Figure 7 Flood simulation effects based on the initial and optimized parameters.